Project of Strategic Interest NEXTDATA

Deliverable D2.6.1
Report on the results of the Pilot Studies

Resp: Antonello Provenzale, CNR-ISAC

Project of Strategic Interest NEXTDATA

D2.6.a - Results of the pilot study: "Water resources in the Himalaya-Karakorum and interaction between monsoon and mid-latitude disturbances"

Prepared by: Elisa Palazzi (CNR-ISAC, Torino)

Contributors:
Jost von Hardenberg (CNR-ISAC, Torino), Antonello Provenzale (CNR-ISAC, Torino), Luca Filippi (CNR-ISAC, Torino), Paolo Cristofanelli (CNR-ISAC, Bologna), Paolo Bonasoni (CNR-ISAC, Bologna), Adnan Tahir (COMSATS Institute, Abbotabad), Elisa Vuillermoz (Ev-K2-CNR, Bergamo), Gian Pietro Verza (Ev-K2-CNR, Bergamo).

This deliverable is structured into three sections, followed by a final part which summarizes the progresses and outcomes of the pilot study during the first year of activity.

The first section describes the study of current and future precipitation in the Hindu-Kush Karakoram Himalaya (HKKH) region that we performed making use of various gridded observational datasets, reanalysis data and the output of one state-of the art Global Climate Model (EC-Earth).

The second section focuses on the western portion of the HKKH domain, namely the Hindu-Kush Karakoram (HKK), and makes use of in-situ meteorological data (in particular precipitation and temperature records) from individual stations spread over the upper Indus basin region to analyse the horizontal and vertical variability of precipitation and temperature in northern Pakistan and their long-term trends at the locations of the individual stations.

The third section describes the synoptic scale circulation affecting northern Pakistan in summer and winter making use of back-trajectory analyses. This section also presents a preliminary study of the western weather pattern tracks from the Atlantic/Mediterranean to the Karakoram region.

1. Precipitation in the Hindu-Kush Karakoram Himalaya: observations and future scenarios

The complex topography, circulation patterns and climatic responses in different parts of the Hindu-Kush Karakoram Himalaya (HKKH) range make a global description of these mountain areas scarcely useful and suggest a division into sub-regions. In this work we consider separately two main areas, the Hindu-Kush Karakoram (HKK) in the west and the Himalaya in the east, which are exposed to different circulations, precipitation patterns and are characterized by different glacier behaviour and dynamics [Bookhagen and Burbank, 2010]. We have defined two domains, shown in Fig. 1.1.1, which contain the main sub-regions of the HKK and Himalaya mentioned above, in the ranges 71°E-78°E/32°N-37°N and

78°E-93°E/25°N-32°N respectively. We analyse the patterns, annual cycle and long-term trends of summer and winter precipitation in the two domains, focusing on mountain areas with elevation higher than 1,000 m above mean sea level. To this end, we use several observational datasets: satellite observations (TRMM 3B42), rainfall archives based on the interpolation on regular spatial grids of sparse in-situ stations data (APHRODITE, GPCC, and CRU datasets), merged satellite-rain gauge data (GPCP climatology), reanalyses (ERA-Interim), and the precipitation provided by an ensemble of simulations of the state-of-the-art global climate model EC-Earth [Hazeleger et al., 2012]. The statistics of the climate model output in the historical period are compared with the climatology provided by the other datasets, to assess how well this global climate model reproduces the observed seasonality and long-term behaviour of precipitation in the two focus regions. Future projections of precipitation trends in terms of rainfall averages and intensity are obtained with two scenarios produced by the model for the twenty-first century, based on the representative concentration pathways "RCP 4.5" and "RCP 8.5" [Moss et al., 2010].

In this study, we define summer to include the months from June to September (JJAS), over which the summer monsoon typically manifests itself over the eastern stretches of the HKKH. Winter includes the months from December to April (DJFMA), due to the duration of the wintertime precipitation in the HKK area.

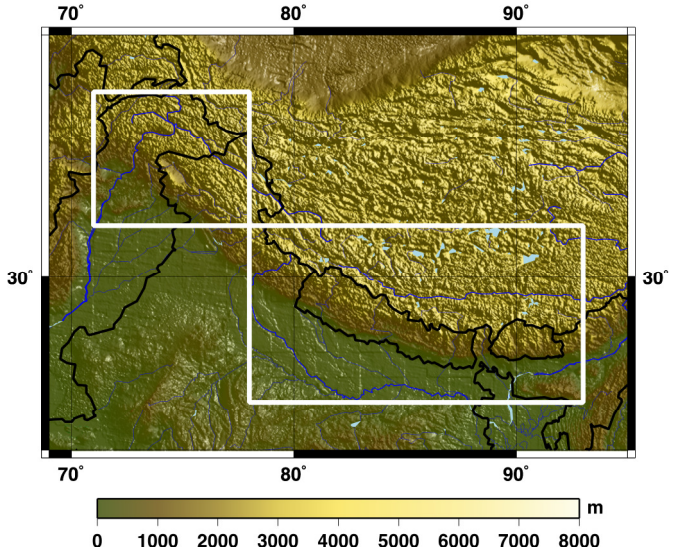

Figure 1.1.1. Map of the study area and of the HKK (West) and Himalaya (East) domains.

The spatial distribution of summer (JJAS) and winter (DJFMA) precipitation over a region which includes the HKKH range, obtained from the APHRODITE, CRU, GPCC, TRMM, GPCP and ERA-Interim datasets and from EC-Earth is shown in Figs. 1.1.2 and 1.1.3, respectively. Precipitation is averaged over the period 1998-2007.

All datasets coherently reproduce the key features of summer and winter precipitation in the HKKH region. During summer (Fig. 1.1.2), precipitation is concentrated over the eastern stretch of the Himalaya and decreases from south-east to north-west along the Himalayan chain. Mountain regions in northern Pakistan are quite dry during summer, reaching a maximum precipitation of about 3-4 mm/day. During winter (Fig. 1.1.3), while the whole Himalayas receive considerably lower precipitation amounts than during summer, the land masses of northern Pakistan receive a water input carried by eastward propagating mid-latitude patterns (also called western weather patterns). Moisture-laden westerly winds are intercepted as they encounter high mountain ranges in northern Pakistan, leading to moisture condensation and precipitation at high altitudes and dry conditions at the interior high plains.

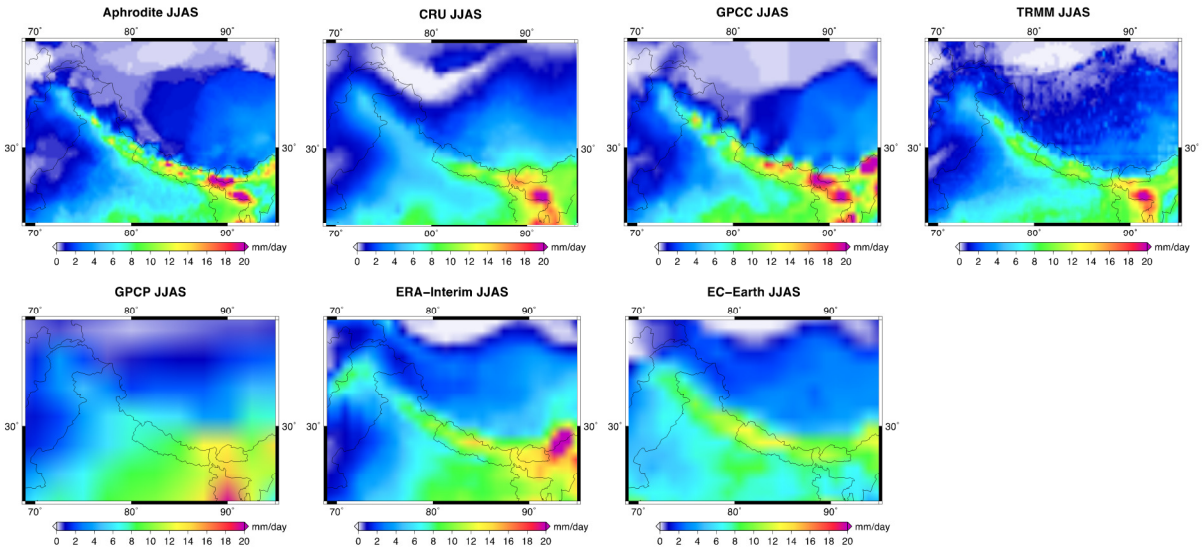

Figure 1.1.2. Multiannual mean (1998-2007) of summer (JJAS) precipitation over the region between 69°-95°E and 23°-39°N from the APHRODITE, CRU, GPCC, TRMM, GPCP, ERA-Interim and EC-Earth model datasets.

Though the key features of the precipitation field over the target area are well represented by all datasets, important discrepancies arise from the different temporal and spatial sampling and resolution and from the specific characteristics of the various products, such as different bias correction, homogenization or interpolation choices. Important differences are observed in winter precipitation over North Pakistan and in summer precipitation over Nepal, two periods which are essential for the hydrologic budget of these two areas. It is also important to point out that while the reanalysis and global climate model data estimate the total precipitation (including snow), the APHRODITE, CRU and GPCC station data and the TRMM 3B42 product provide rainfall estimates. In areas with sparse station coverage, the GPCC, APHRODITE, and CRU datasets interpolate grid-point values from the nearest few available stations, introducing a significant element of uncertainty.

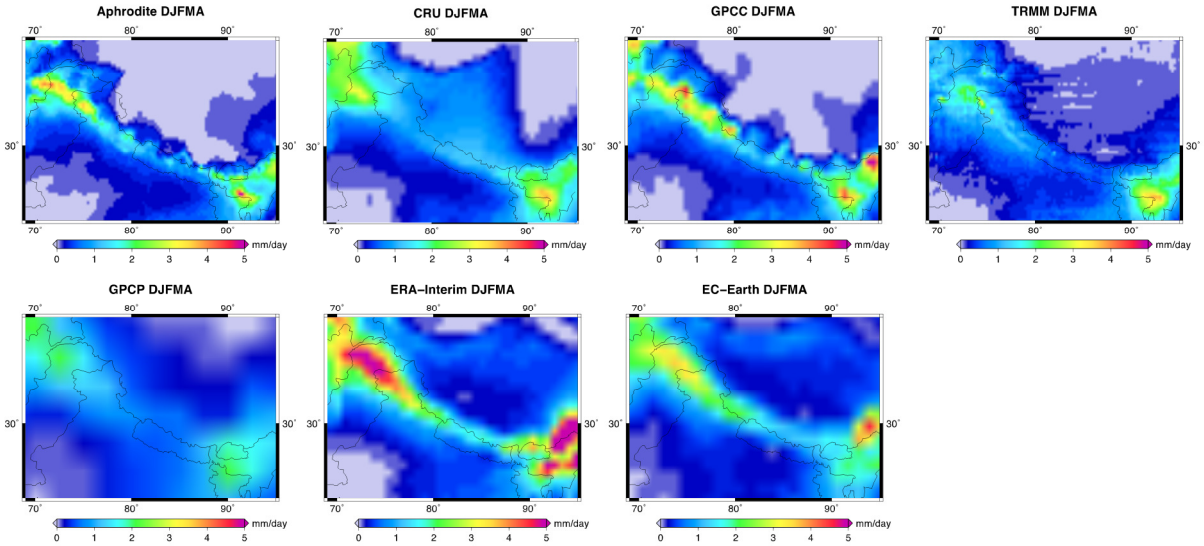

Figure 1.1.3. Multiannual mean (1998-2007) of winter (DJFMA) precipitation over the region between 69°-95°E and 23°-39°N from the APHRODITE, CRU, GPCC, TRMM, GPCP, ERA-Interim and EC-Earth model datasets.

The annual cycle of precipitation averaged over the high-elevation regions of the HKK domain (solid lines) and of the Himalaya domain (dashed lines) from the APHRODITE, CRU, GPCC, TRMM, GPCP, ERA-Interim datasets and the EC-Earth model is shown in Fig. 1.1.4. The mean annual cycle of precipitation is calculated as the average over the time period 1998-

2007 which is common to all datasets. All datasets give a similar picture of the monthly climatology of precipitation, with a bimodal distribution in the HKK and a unimodal distribution in the Himalaya. In fact, the figure is consistent with the two principal sources of precipitation in the whole HKKH range. The monsoon represents the dominant source in terms of total amounts of precipitation delivered, bringing storm systems from the south to the Himalayan range in the period from late June through September, with a maximum in July, coherently reproduced by all datasets. The precipitation peak in July is lower for APHRODITE and TRMM (around 5 mm/day) than for GPCP (around 5.5-6 mm/day), CRU and GPCC (6.5 mm/day) and ERA-Interim (around 10 mm/day). In the HKK domain a further source of precipitation occurs in winter/early spring (February/April), which is known to be associated with midlatitude westerly weather systems. ERA-Interim overestimates precipitation compared to the other datasets. The wintertime peak, whose timing is anyway consistent with observations, is about 4 mm/day. Precipitation for EC-Earth in the Himalaya is in better agreement with the observations than ERA-Interim. In the HKK domain, EC-Earth precipitation is higher than the satellite/in-situ derived observations, but still lower than ERA-Interim. Both in-situ station data and satellite estimates have difficulties in detecting the snow component of precipitation. This could lead to an underestimation of precipitation, particularly in snow-rich areas such as the HKKH and especially in winter. Even if some of the observational, satellite and merged datasets considered here have been treated for bias correction, this issue may contribute to the higher precipitation values found for ERA-Interim and EC-Earth. To explore this point, we report in Fig. 1.1.4 the contribution of liquid-only precipitation for EC-Earth and ERA-Interim (lines with stars), obtained by removing the snowfall flux from the total precipitation. An improvement is indeed observed for ERA-Interim, which gets closer to the observations in winter in HKK. EC-Earth displays an overall lowering of precipitation amounts after removing snowfall. In the HKK domain in winter the liquid precipitation component becomes significantly lower than the observations. One possibility is that measured precipitation (especially from rain gauges) includes a partial contribution from snow (typically, snow underestimates are very variable and can easily reach a factor of 2 or more, see Rasmussen et al. [2012]). On the other hand, the model may overestimate snow with respect to rainfall, particularly during winter. It is indeed known that EC-Earth has, globally, a cold bias [Hazeleger et al., 2012], which could cause a wrong partition between snow and rain, probably associated with a model overestimation of snow cover and surface albedo during winter and spring [Dutra et al., 2010].

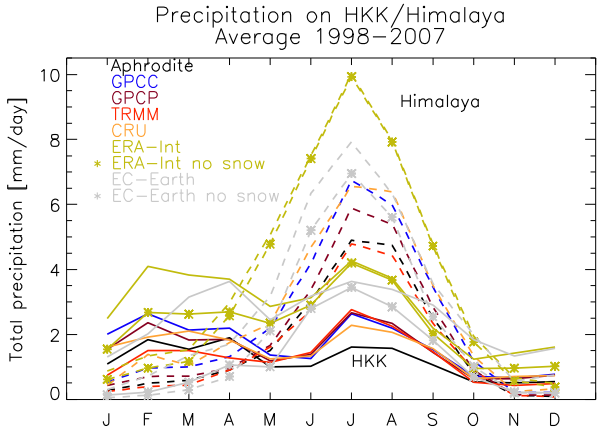

Figure 1.1.4. Monthly climatology of precipitation (averaged over the period 1998-2007) for the HKK domain (solid lines) and the Himalaya domain (dashed lines), for the APHRODITE, GPCC, GPCP, TRMM, CRU, ERA-Interim and EC-Earth datasets. The lines marked with stars indicate liquid precipitation only (obtained subtracting the snowfall flux from total precipitation for ERA-Interim and EC-Earth).

Time series of yearly average winter and summer precipitation for the HKK and Himalayan sub-regions are shown in Fig. 1.1.5. The figure shows that the elevated regions of the HKK domain receive comparable amounts of precipitation during summer and winter, while in the Himalaya summer precipitation largely exceeds winter precipitation. APHRODITE has

very high correlation values with GPCC and GPCP in both seasons, both for the Himalaya and for HKK. The extremely high correlations found between GPCC and GPCP, in both summer ($r > 0.85$) and winter ($r > 0.84$), could be expected since GPCC data are the in-situ component of the GPCP dataset. Interestingly, Fig. 1.1.5 shows that despite being highly correlated, the GPCC and GPCP datasets do not always agree in terms of precipitation amounts in both domains. This could reflect the local effect of bias adjustments in the datasets. The CRU data generally present lower correlations in the Himalaya than in the HKK region, possibly due to a different coverage in terms of stations in the two areas. The correlations of TRMM measurements with all in-situ based datasets are higher in winter than in summer (except with CRU). It is important to point out that some of these low correlations are probably due to the fact that most raingauges are located in the valley bottom, while highest rainfall amounts occur at higher elevation. It is exactly this signal that the remote sensing data are most sensitive to [Bookhagen and Burbank, 2006; Barros et al., 2000]. ERA-Interim data have a generally good correlation with the main in-situ and merged observational datasets during winter, while they correlate less in summer, particularly for the Himalaya. The precipitation of ERA-Interim has a significant high bias compared to the observational datasets.

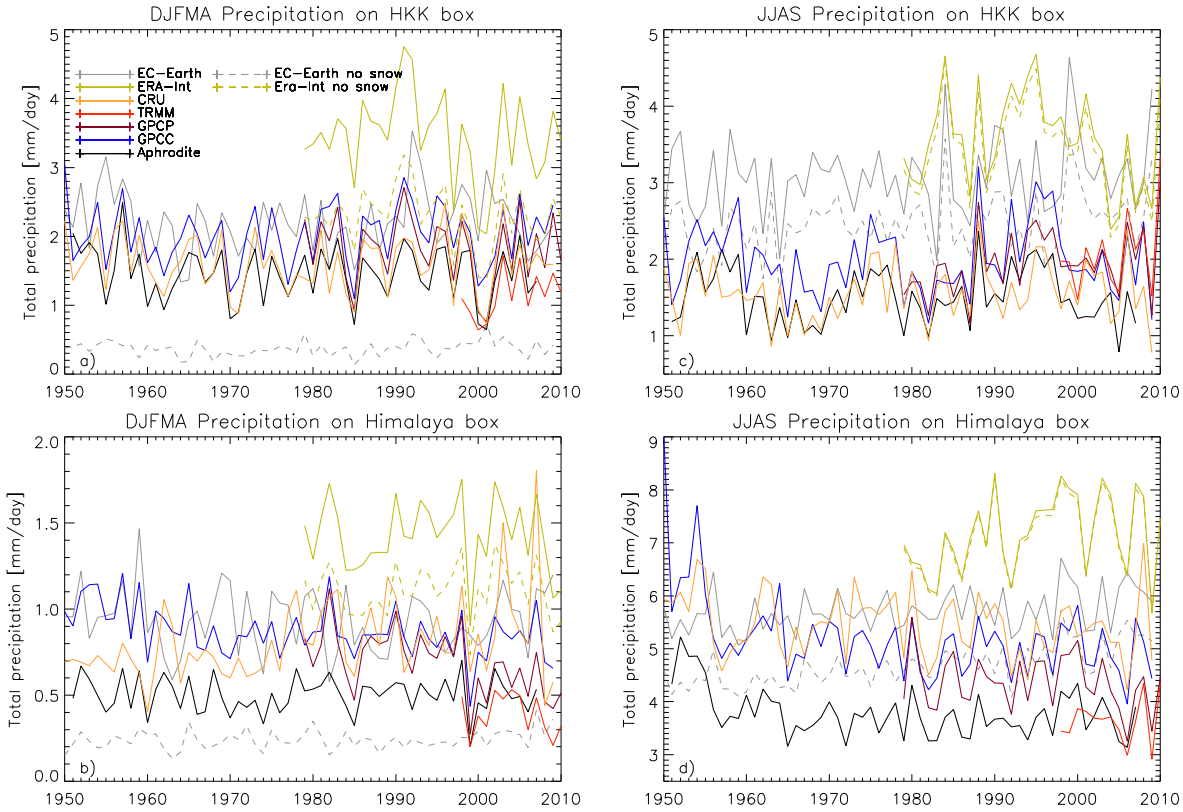

Figure 1.1.5. Time series of precipitation over the HKK domain (a,c) and the Himalaya domain (b,d) during DJFMA (a,b) and JJAS (c,d) for the APHRODITE, GPCC, GPCP, TRMM, CRU, and ERA- Interim datasets (from 1950 onwards), and from the EC-Earth model, shown as the grey line. The dashed lines are for liquid precipitation (that is, after removing snow), for ERA-Interim and for the EC-Earth model.

The interannual fluctuations of EC-Earth precipitation, shown as the grey lines in Fig. 1.1.5 cannot be correlated with observations, since the model runs in climate mode (while the model attempts to reproduce the properties of real climate in a statistical sense, there will be no exact agreement with observations in any particular year). For the HKK domain during summer we find a high bias of almost 1 mm/day compared to observations, similar to that observed for ERA-Interim. It is possible that this bias is of dynamical origin and linked with an excessive summer monsoonal flow, with associated precipitation, extending to this

region. As noted previously, some of the biases between EC-Earth or ERA-Interim and the observations may be linked to difficulties in measuring the snow component of precipitation. For completeness, we report the contribution of liquid-only precipitation for EC-Earth and ERA-Interim, shown with the dashed lines in Fig. 1.1.5. The same considerations discussed above for seasonality apply also in this case.

Table 1.1.1 summarizes the values of JJAS and DJFMA precipitation trends obtained from the various datasets for HKK and Himalaya. Note that the table also shows, for each dataset, the period of time over which trend calculation is performed to emphasize that trends from the various sources refer to different periods. Starred entries in the table indicate the ERA-Interim and EC-Earth liquid precipitation data. Data in bold style refer to trend values that are statistically significant at the 95% confidence level (the corresponding p-value is indicated in brackets).

Table 1.1.1. Precipitation trends (in mm/day/year) in the HKK and Himalaya during summer (JJAS) and winter (DJFMA) for the various datasets (in parentheses the years over which trends have been calculated). Bold figures are significant at the 95% level (p-value indicated in brackets).

	JJAS		DJFMA	
	Himalaya	HKK	Himalaya	HKK
APHRODITE (1951-2007)	**-0.010(p=0.001)**	0.0	0.0	-0.003
CRU (1950-2009)	-0.008	0.002	**0.005(p=0.004)**	-0.001
GPCC (1950-2009)	**-0.021(p=0.001)**	0.0	**-0.004(p=0.000)**	0.002
TRMM (1998-2010)	0.015	0.057	-0.006	0.041
GPCP (1979-2010)	-0.012	**0.017(p=0.045)**	**-0.010(p=0.001)**	-0.007
ERA-Interim (1979-2010)	0.027	-0.011	-0.002	-0.012
EC-Earth (1950-2009)	**0.008(p=0.002)**	0.005	-0.001	0.0
∗ ERA-Interim (1979-2010)	0.027	-0.011	0.0	-0.007
∗ EC-Earth (1950-2009)	**0.014(p=0.000)**	**0.007(p=0.027)**	**0.001(p=0.050)**	0.001

None of the spatially-averaged precipitation time series provides statistically significant evidence of long-term trends in HKK in winter. In HKK during summer, GPCP provides a statistically significant increasing trend of 0.017 mm/day/year and so does EC-Earth (0.007 mm/day/year).

Archer and Fowler [2004] discussed seasonal precipitation trends in the Karakoram region and found an upward trend in winter precipitation in the period 1961-1999, statistically significant at three out of seventeen stations they analyzed (Skardu, 2,210 m; Shahpur, 2,012 m; Dir, 1,425 m; see also Section 2 of this document). It is interesting that no such trend emerges from the analysis of the ensemble of datasets considered here.

In the Himalaya during winter, the CRU data indicate a statistically significant increasing trend of about 0.005 mm/day/year while GPCC gives an opposite trend of about -0.004 mm/day/year; both trends are evaluated over the time period 1950-2009. GPCP gives a statistically significant decreasing trend of -0.010 mm/day/year in the same region and season but computed on a shorter period of time (1979-2010). In the Himalaya during summer the CRU data indicate a decreasing precipitation trend (-0.008 mm/day/year), which is not significant at the 95% confidence level (p=0.1). On the other hand, a statistically significant trend in summer precipitation in the Himalaya is provided by two out of the three longest observational datasets (APHRODITE and GPCC, covering almost the same period of time), corresponding to a decrease of about, respectively, -0.010 mm/day/year and -0.021 mm/day/year. Unlike the observations, EC-Earth indicates an increasing trend of monsoon precipitation in the Himalaya domain in the period 1950-2005. This could be due to the fact

that the countering effects of the recent increases of atmospheric aerosol resulting from the combustion of fossil fuels in Asia [Ramanathan et al., 2005] is not correctly reproduced and/or to an improper representation of aerosols in this climate model. It is worth mentioning that other studies suggest that the observed drying trend over the Himalayas in summer could be linked to a larger input of aeolian dust from the west, associated to changes in the wind field in recent decades (Dr. Conroy, personal communication), a hypothesis we intend to explore in the near future.

We extend the individual EC-Earth simulation discussed above and consider an ensemble of independent realizations created, under the same historical and future forcing conditions, by the participants in the EC-Earth consortium (see http://ecearth.knmi.nl/). Figure 1.1.6 shows the time series of precipitation (after filtering with a 5-years running mean) from the resulting eight-member ensemble in the historical period (1850-2005) and for the future (2006-2100) in the RCP 4.5 scenario, for the two sub-regions of HKK (panels a,b) and Himalaya (c,d), averaged over winter (a,c) and summer (b,d). In order to highlight the interannual variability of the model precipitation, we report the EC-Earth simulation used above with a thick black line. Figure 1.1.7 shows the same as Fig. 1.1.6, but for the more extreme RCP 8.5 scenario. As already discussed, Figs. 1.1.6 and 1.1.7 show that in Himalaya during summer (panel d), EC-Earth indicates an increasing trend of precipitation in the period 1950-2009. Seven out of eight EC-Earth members actually give a statistically significant trend which corresponds to an increase in average precipitation rate between 0.005 and 0.010 mm/day/year.

The increasing trend in summer precipitation over the Himalaya is projected to continue under the most extreme RCP 8.5 scenario (panel d of Fig. 1.1.7). All eight EC-Earth members predict a statistically significant trend corresponding to an increase of about 0.008 to 0.014 mm/day/year (average increase of about 0.8 to 1.2 mm/day in the period 2006-2100). In the RCP 4.5 scenario (panel d of Fig. 1.1.6), the increasing trend indicated by the model in the historical period continues till about 2050, when it stabilizes and a slight decrease starts. No statistically significant trend is found in the Himalaya in summer under the RCP 4.5 scenario. In the Himalaya during winter, one out of eight EC-Earth members provides a statistically significant increase in precipitation (0.08 mm/day/(95 years)) in the RCP 4.5 scenario, and another member shows a trend in future precipitation in the RCP 8.5 scenario corresponding to an increase of 0.16 mm/day/(95 years). Three (five) out of eight EC-Earth members give a statistically significant increasing trend in winter precipitation in the HKK of about 0.3 to 0.4 (0.4 to 0.7) mm/day/(95 years) under the RCP 4.5 (RCP 8.5) scenario. No statistically significant precipitation trend is found during summer in the HKK in the RCP 4.5 scenario, while in the RCP 8.5 scenario, two members give an increase in summer precipitation of about 0.5 mm/day/(95 years).

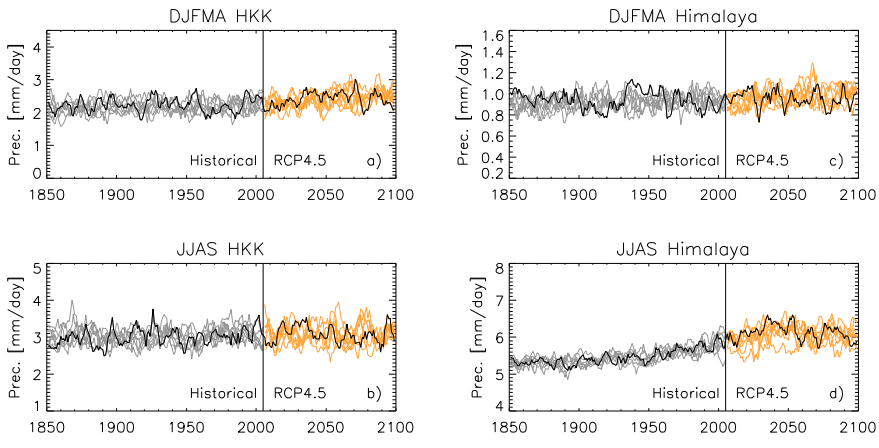

Figure 1.1.6. Time series of precipitation over HKK (a,b) and the Himalaya domain (c,d) during DJFMA (a,c) and JJAS (b,d) from the eight realizations of the EC-Earth model ensemble for the historical period (1850-2005, grey lines) and from 2006 to 2100 (orange lines) in the the RCP 4.5 scenario.

We further explore the trend in precipitation found for the Himalaya in summer in the two future scenarios. The analysis of daily time series shows that this trend is associated with changes in the distribution of intense precipitation episodes. In Fig. 1.1.8 (panels a and e) we report the evolution of the amplitude distribution of daily precipitation from 1850 to 2100 in the Himalaya during summer, reporting the 99th, 95th, and 90th percentile lines.

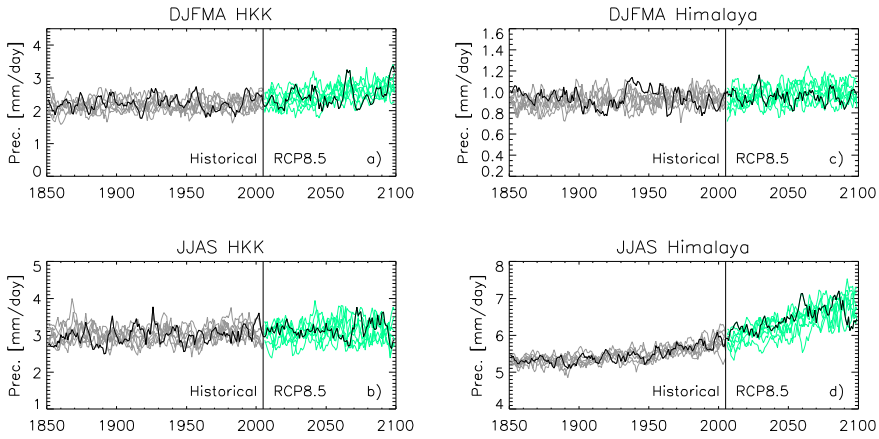

Figure 1.1.7. Same ad Fig. 1.1.6, but for the RCP 8.5 scenario.

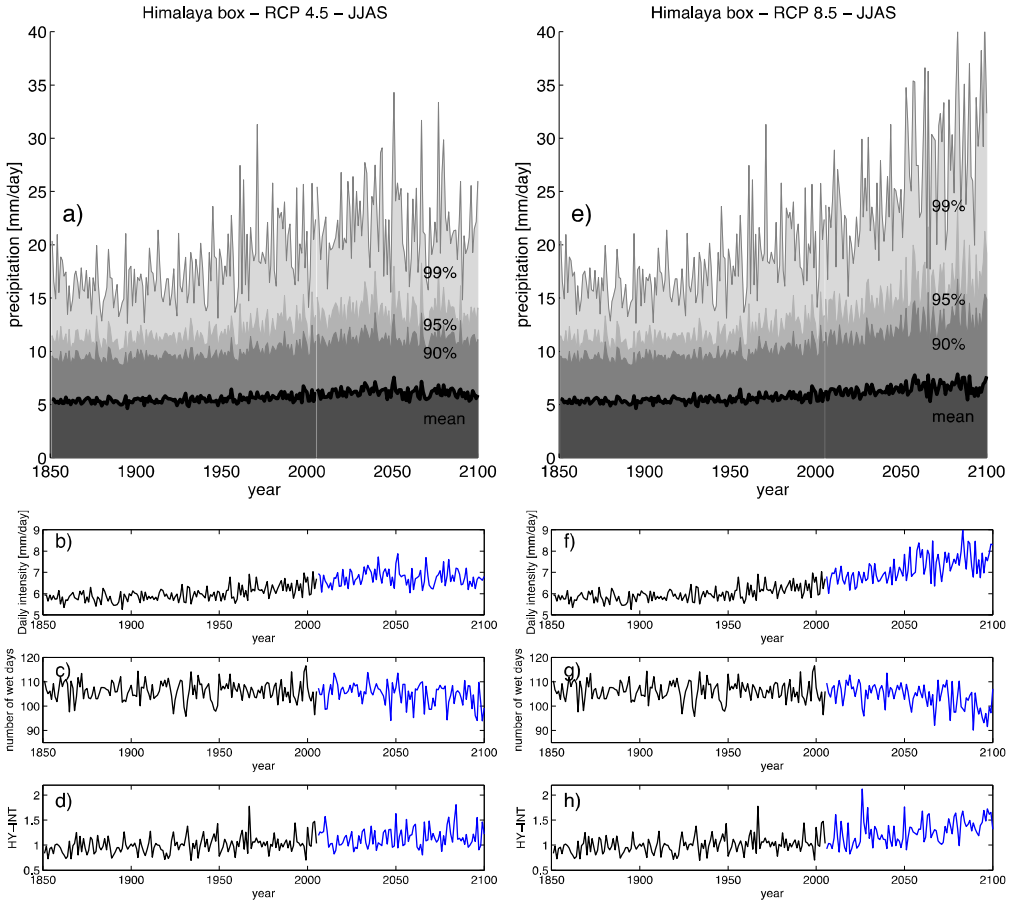

Figure 1.1.8. Precipitation statistics for EC-Earth. Time series of a,e) average daily precipitation (black thick line) and precipitation above the 90th, 95th, and 99th percentiles (shaded regions); b,f) daily precipitation intensity; c,g) number of days with precipitation larger than 1 mm/day (wet days); d,h) the hydroclimatic index HY-INT, for the Himalaya domain during summer. Left: RCP 4.5; Right: RCP 8.5 scenario.

For both scenarios, the increasing trend in summer precipitation over the Himalaya is associated with an increasing trend in precipitation extremes. For the RCP 8.5 scenario, in particular, daily precipitation intensity (f) is projected to increase through the twenty-first century, in line with the increase in precipitation extremes (□1.3 mm/day over the period 2006-2100). The number of wet days during the warm season (g) shows a significant decreasing trend (-□8 days over 2006-2100). This is in line with climate projections at the global scale, which indicate for the twenty-first century an increase in precipitation intensity and number of dry days in response to increased greenhouse gas concentrations, although with pronounced regional variability [Solomon et al., 2007]. The RCP 4.5 scenario presents a similar picture, with an increase followed by stabilization of precipitation intensity at mid-21st century (b). The number of wet days does present a weak, but significant trend (-4.5 days in 2006-2100, panel c). We also discuss changes in hydroclimatic intensity computing the "HY-INT" index introduced by Giorgi et al. [2011]. HY-INT is defined as the product of the average precipitation intensity in mm/day and the average dry spell length in days, here both normalized to their values in the period 1850-2005. The HY-INT index is sensitive to increases in both quantities which define it and has been found to be an ubiquitous signature, in several regions of the world, of twenty-first century global warming. The evolution of the index is reported in Fig. 1.1.8 (panels d,h). We find a significant positive trend in HY-INT in the Himalaya for the RCP 8.5 scenario (0.38 in the period 2006-2100), indicating a trend towards more episodic and intense monsoonal precipitation. No significant trend in the 21st century can be found for HY-INT in the RCP 4.5 scenario simulated by EC-Earth. The projected increase of HY-INT in the RCP 8.5 scenario should however be taken with caution, both because no significant trend is visible in the more moderate RCP 4.5 scenario and because most climate models indicate an intensification of the hydrological cycle in the Himalaya during summer also in the last fifty years, which is not supported by the observations.

Please see Palazzi et al, (2013), for details about this study.

2. Climatic characterization of the Baltoro glacier area and northern Pakistan from in-situ stations

For long time, the meteorological measurements in the upper Indus basin have been mostly confined to valley locations, far from the most active hydrological zones where maximum snowfall and accumulation occur [Young and Hewitt, 1990]. The lack of long-term monitoring programmes for this area and the sparseness of near glacier high-elevation data represent one of major issues of the Karakoram meteorology and climate studies. In spite of these difficulties, in the recent years, much attention has been focused on the Baltoro glacier. One of the most important water reserves of the Karakoram, this glacier is an essential Pakistan water supply in the dry season. In the framework of the recent Stations at High Altitude for Research on the Environment (SHARE) programme (http://www.evk2cnr.org/cms/en/share/project/intro) of the Italian National Research Council (CNR), the Ev-K2-CNR Committee has established and maintains, in collaboration with the PMD, two Automatic Weather Stations (AWS) for the monitoring of the Baltoro glacier, located at Askole (3,015 m a.s.l.) and Urdukas (3,926 m a.s.l.). A third station collecting the meteorological parameters in the Baltoro was installed in summer 2011 at Concordia (4,700 m a.s.l.).

We have analysed the meteorological data collected at the Askole and Urdukas stations during the first five years of operation (from 2004 to 2009), to provide a general characterisation of the meteorology of the region surrounding the two stations. These data

are complemented by longer time series of precipitation and temperature obtained by various other in-situ stations, managed by the Pakistani Meteorological Department (PMD) and the Water and Power Development Authority (WAPDA) agencies, spread over northern Pakistan and located at different altitudes ranging from 1,250 to 4,710 m a.s.l.. We exploit the data availability from all in-situ stations (totally sixteen AWS) to 1) make analyses of temperature and precipitation seasonal trends in the upper Indus basin (UIB) region; 2) assess to which extent individual records of temperature and precipitation are representative of the entire UIB region we have investigated and 3) explore the altitudinal variability in temperature and precipitation, which is essential to understand the hydrometeorology of this area.

The geographical distribution of the in-situ stations employed in our analysis is shown in Fig. 1.2.1 and their principal characteristics –temporal length and resolution of the data sets, altitude, latitude and longitude coordinates – are resumed in Table 1.2.1. A brief description of the in-situ stations in the Baltoro is given in section 2.1, while the WAPDA and PMD are described in section 2.2.

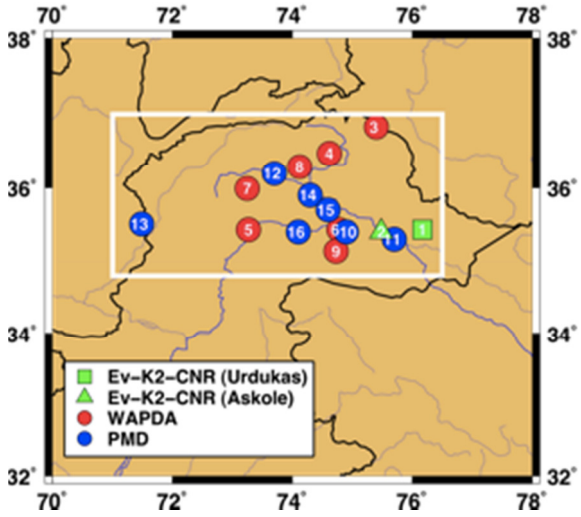

Figure 1.2.1. Geographical distribution of the sixteen in-situ stations employed in this study: Ev-K2-CNR (green), WAPDA (red) and PMD (blue) AWS (refer to Table 1.2.1 for the station numbering).

Table 1.2.1 Temporal range, elevation, latitude and longitude coordinates of the in-situ stations considered in this study, along with the temporal resolution of the measured data and their source/agency.

Stations	Time period	z (m asl)	Lat (°N)	Lon (°E)	Resolution	Agency
1. Urdukas	2004-2008	3,962	35.43	76.17	Hourly	Ev-K2-CNR
2. Askole	2005-2009	3,015	35.40	75.48	Hourly	Ev-K2-CNR
3. Khunjerab	1999-2008	4,710	36.83	75.40	Daily	WAPDA
4. Ziarat	1999-2008	3,669	36.47	74.62	Daily	WAPDA
5. Yasin	1999-2008	3,150	35.43	73.27	Daily	WAPDA
6. Rama	1999-2008	3,000	35.43	74.79	Daily	WAPDA
7. Ushkore	1999-2008	2,970	35.99	73.25	Daily	WAPDA
8. Naltar	1999-2008	2,810	36.29	74.12	Daily	WAPDA
9. Rattu	1999-2008	2,570	35.14	74.73	Daily	WAPDA
10. Astore	T (P):1954-2000 (2007)	2,394	35.4	74.9	Monthly	PMD
11. Skardu	T (P):1953-2000 (2007)	2,210	35.3	75.7	Monthly	PMD
12. Gupis	T (P):1955-2000 (2007)	2,156	36.2	73.7	Monthly	PMD
13. Chitral	T (P):1965-2000 (2007)	1,498	35.51	71.49	Monthly	PMD
14. Gilgit	T (P):1945 (1951)-2007	1,460	35.9	74.3	Monthly	PMD
15. Bunji	T (P):1953-2000 (2007)	1,372	35.7	74.6	Monthly	PMD
16. Chilas	T (P):1953-2000 (2007)	1,250	35.4	74.1	Monthly	PMD

2.1 Automatic Weather Stations in the Baltoro Glacier

Two automatic stations for the monitoring of the standard meteorological parameters in the Baltoro glacier were installed at the Urdukas campsite (35°43'N, 76°17'E) and in the Askole village (35°40'N, 75°48'E), about 45 km away each other, in June 2004 and August 2005, respectively. Urdukas is located in the middle of the Baltoro glacier on the trek way to Concordia and the AWS was installed at 3,962 m a.s.l. on a moraine ridge close to the left margin of the glacier. Askole is the last village on the route to the Baltoro glacier and mount K2, at an average elevation of 3,000 m a.s.l.. The village is on the right side of the valley and north of the main river, on a moraine highland with small inclination toward the Braldu river; the AWS is located on the lower, southern part of the moraine, near its edge above the river. The two stations provide measurements of the standard meteorological parameters (including precipitation, air temperature, relative humidity, air pressure, incoming short wave radiation, wind speed and direction) carried out following the WMO guidelines [Zahumenský, 2004; WMO, 2008]. The raw data consist of hourly mean values for all variables except for precipitation, for which hourly-accumulated data are supplied. The collecting sensors are mounted at heights of 2 meters and 5 meters (for wind measurements) on the same mast. Unless exceptional situations or emergencies happen, the data are downloaded twice every year (in spring and autumn) by specialized personnel and immediately checked on-site. Data validation is subsequently performed following the international guidelines defined within the Coordinated Energy and water cycle Observations Project (CEOP, http://www.eol.ucar.edu/projects/ceop/dm/documents/refdata_report/data_flag_definitions.html).

2.2 In-situ data for northern Pakistan: WAPDA and PMD stations

We consider the precipitation and temperature data collected by fourteen in-situ meteorological stations operated by the PMD and WAPDA agencies of Pakistan.

- PMD maintains stations with standard meteorological measurements, with earliest data in 1950s. Stations established by the PMD are mainly located in valleys at relatively low elevations. In this study we analyze about 50-years of monthly-mean, maximum and minimum temperature and monthly-accumulated precipitation from seven stations (see Fig. 1.2.1, blue circles) located at altitudes between 1,250 m a.s.l. (Chilas) and 2,394 m a.s.l. (Astore), as also indicated in Table 1.2.1.

- WAPDA also maintains a wide network of in-situ meteorological and hydrological stations in the ablation zone of the Upper Indus Basin cryosphere, but with shorter temporal length than the PMD stations. In this study, we use ten years (1999-2008) of daily-mean, maximum and minimum temperature and daily-accumulated precipitation from seven stations located at different altitudes covering a range from 2,570 m a.s.l. (Rattu) to 4,710 m a.s.l. (Khunjerab) (see Fig. 1.2.1 and Table 1.2.1 for details).

2.3 Meteorological characterization of the Baltoro glacier

Figure 1.2.2 shows the daily-averaged time series of 2-metres temperature (a), relative humidity (c) and incoming short wave radiation (d), and the time series of daily-accumulated precipitation (b) at the Askole (black) and Urdukas (gray) stations. The right-column plots (e to h) show, for each measured variable, the time series of the fraction of "good" quality data per month, evaluated according to the CEOP guidelines. Data flagged as "dubious" and "bad" have been excluded from our analyses. Labels "J, A, J, O" above the years in the horizontal axis of each plot stand for "January, April, July, October".

Figure 1.2.2 indicates that:
- surface air temperature at Askole and Urdukas shows a clear seasonal cycle and a spatial variability primarily dependent on the elevation of the two stations;
- precipitation data reveal the persistence of semiarid conditions in the region surrounding the two AWS; on the other hand, wintertime precipitation is not accounted for in these data;
- the lack of meaningful correlation between temperature and relative humidity measured at the two stations confirms that the HKK region is not under the prevalence of a monsoon-controlled dynamics.

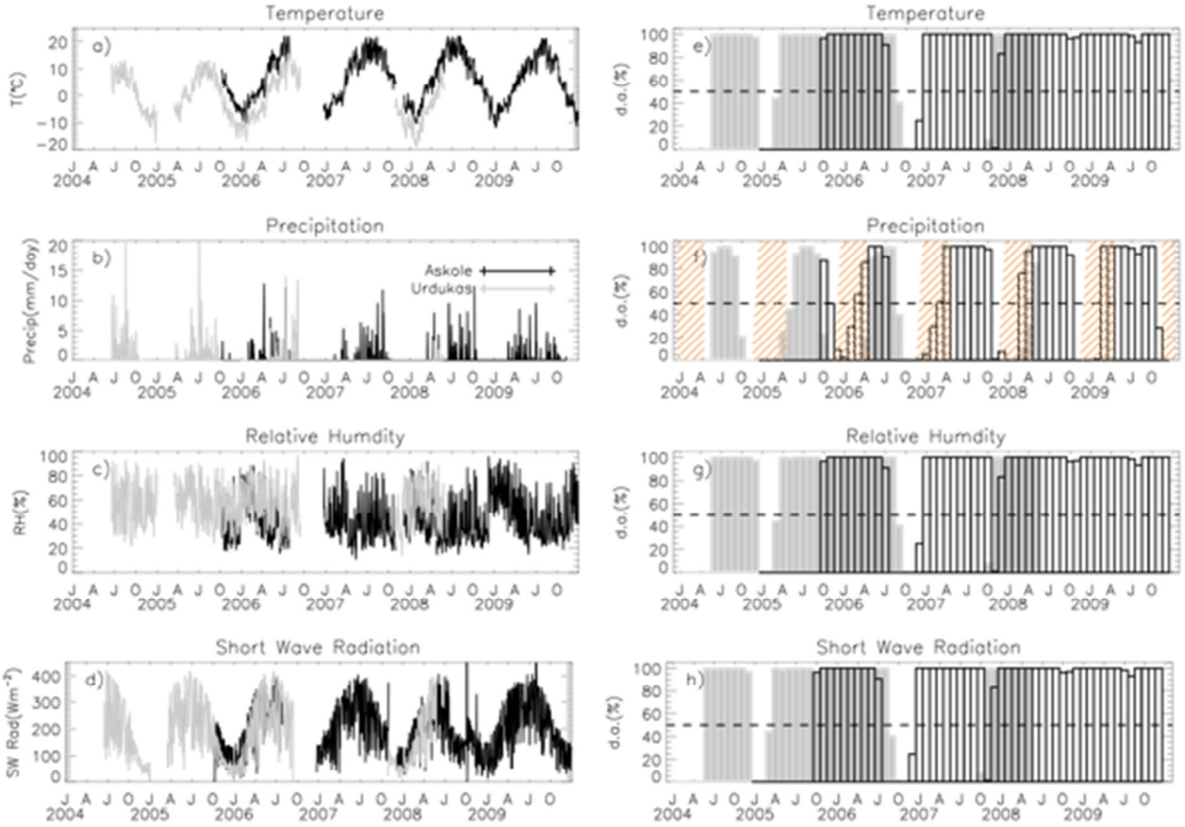

Figure 1.2.2. (Left) Daily time series of temperature (a), precipitation (b), relative humidity (c), and short wave radiation (d) and (right) fraction of good quality data per month ("d.a." in the y-axis stands for "data availability") at the two stations for each parameter (e to h). The dashed horizontal line in the right-column plots indicates the limit of 50% of good quality data; the lined regions in panel (f) identify winter seasons (from December to April).

The datasets at both stations show some discontinuities, generally due to occasional sensor or datalogger malfunctioning. As for precipitation, however, most data gaps occurred during winter and early spring, when the collection efficiency lowers considerably owing to the difficulty in measuring precipitation in solid form, mostly caused by the strong interference of wind with the automatic measurement devices, one of the most serious issues in measuring precipitation in mountain environments [e.g., Winiger *et al*., 2005]. Wind speed is indeed considered the most important environmental factor contributing to the systematic underestimation of snow in high-altitude regions, and the measurement errors for solid precipitation can range from 20% to 50% due to undercatch in windy conditions [Rasmussen *et al*. 2012].

Figure 1.2.3 shows the hourly wind intensity (filled lines, left y-axis) and wind direction (cross symbols, right y-axis) measured at the Askole (black) and Urdukas (grey) stations for a median day calculated over the whole working period of each station. A clear mountain

regime is discernible at the two sites. In late morning/early afternoon, warm air masses move upward (anabatic, up-valley winds) and eastward (since the two stations are located west of the Baltoro glacier). This path is reversed during the afternoon (katabatic, down-valley winds) when masses of cold and dense air drain down the high-elevation areas of the Baltoro. As expected, the anabatic, thermally-induced winds display slightly higher intensity values than the katabatic, gravity-induced winds. There is a general agreement between the characteristics of wind speed and direction at both sites: the two variables are positively correlated and the correlation coefficient, evaluated on the median day is 0.93 at Askole and 0.88 at Urdukas. Peak wind speed values at the two sites are also of particular interest for, among other reasons, the safety and maintenance of the instrumentation installed there. The peak values of wind intensity measured at Askole and Urdukas are, respectively, ~9.8 ms^{-1} and 10.7 ms^{-1} in summer, and 8.8 ms^{-1} and 12.7 ms^{-1} in winter; these values are much higher than the maxima of median wind speed shown in Fig. 1.2.3.

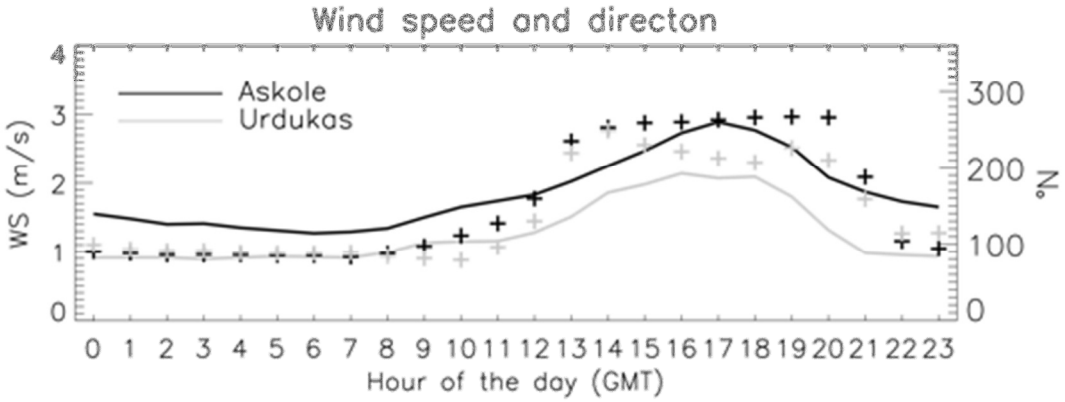

Figure 1.2.3. Wind direction (right axis, cross symbols) and intensity (left axis, filled lines) at the Askole (black) and Urdukas (gray) AWS evaluated for the median day

2.4 Precipitation and temperature trends in the UIB region (1950-2000)

The precipitation and temperature data measured at the seven PMD stations, providing the longest records among the ones we have employed in this study, have been analysed to calculate long-term climatic trends in the upper Indus basin region. A summary of the results for annual and seasonal trends in mean temperature and total precipitation is provided in Table 1.2.2a, while Table 1.2.2b shows the trends in annual, summer and winter minimum and maximum temperature. Bold figures indicate statistically significant trends (at the 95% confidence level, $p<0.05$).

Our analysis indicates that almost all records show summer (JJAS) cooling in the time period from about 1950 to 2000, statistically significant at three out of six stations (Gupis, Gilgit and Bunji with a trend of, respectively, -0.38 °C/decade, -0.34 °C/decade, and -0.79 °C/decade). In contrast, in winter (DJFMA) a statistically significant warming of the mean temperature in the same period of time is seen at Skardu, Chitral and Chilas, with trends of 0.29, 0.26, and 0.17 °C/decade, respectively. Five out of seven stations experienced an increasing trend in winter precipitation (from about 1950 to 2007), though it was statistically significant only at the Gupis station (~0.15 mm/day/decade). Summer precipitation also increased in that period everywhere except at Gilgit; three stations exhibited a statistically significant increasing trend (~0.13 mm/day/decade at Gupis, and ~0.06 mm/day/decade at Bunji and Chilas). Overall decline in summer temperature and increase in winter precipitation derived from our analysis are consistent with the studies performed by Archer and Fowler (2004) and Fowler and Archer (2006). Trends are less evident in the mean temperature series shown in Table 1.2.2a than in the minimum and maximum records (Table 1.2.2b), because of differences in

the long-term behaviour of maximum and minimum temperature series compared to mean temperature series.

Table 1.2.2a. Annual, summer and winter averaged temperature and total precipitation trends (in °C decade^{-1} and mm day^{-1} decade^{-1}, respectively) at the seven PMD stations. The time interval over which the trend of both variables is calculated is also reported.

	Tmean trend (°C/decade)				Total Precipitation trend (mm/day/decade)			
Stations	Time	Annual	JJAS	DJFMA	Time	Annual	JJAS	DJFMA
Astore	1954-2000	0.08	-0.08	0.14	1954-2007	- 0.05	0.02	-0.05
Skardu	1953-2000	**0.19**	0.02	**0.29**	1952-2007	0.0	0.01	0.04
Gupis	1955-2000	-0.13	**-0.38**	-0.03	1955-2007	**0.11**	**0.13**	**0.15**
Chitral	1965-2000	0.07	-0.19	**0.26**	1965-2007	0.02	0.03	-0.03
Gilgit	1945-2007	-0.20	**-0.34**	-0.02	1951-2007	-0.01	-0.02	0.0
Bunji	1953-2000	**-0.37**	**-0.79**	-0.05	1953-2007	0.02	**0.06**	0.01
Chilas	1953-2000	0.12	-0.06	**0.17**	1953-2007	0.02	**0.06**	0.0

Table 1.2.2b. Annual, summer and winter minimum and maximum temperature (in °C decade^{-1}) at the seven PMD stations.

		Tmin trend (°C decade^{-1})			Tmax trend (°C decade^{-1})		
Stations	Time	Annual	JJAS	DJFMA	Annual	JJAS	DJFMA
Astore	1954-2000	0.09	-0.07	0.17	0.07	-0.08	0.08
Skardu	1953-2000	-0.06	**-0.29**	0.14	**0.45**	**0.33**	**0.47**
Gupis	1955-2000	**-0.44**	**-0.72**	**-0.24**	0.16	-0.05	0.18
Chitral	1965-2000	**-0.21**	**-0.37**	0.0	**0.35**	0.0	**0.51**
Gilgit	1945-2007	**-0.70**	**-0.87**	**-0.49**	0.28	0.15	**0.34**
Bunji	1953-2000	**-0.56**	**-0.95**	**-0.18**	**-0.18**	**-0.65**	0.10
Chilas	1953-2000	**0.25**	0.03	**0.37**	-0.02	-0.14	-0.03

2.5 Regional correlation of temperature and precipitation time series

In order to assess the spatial coherence of temperature and precipitation in northern Pakistan, we have calculated the seasonal (JJAS and DJFMA) correlation between the records collected at the PMD stations and between the records collected at the WAPDA stations, separately. Correlation matrices for temperature and precipitation, drawn up between the seven WAPDA stations (for the time period between 1999 to 2008) and the seven PMD stations (1965-2000), are presented in Tables 1.2.3a (WAPDA) and 1.2.3b (PMD). Summer (winter) data are displayed above (below) the diagonal, and the correlation coefficients for precipitation are reported in brackets. Statistically significant correlations (at the 95% confidence level) are shown in italic bold style.

Table 1.2.3a. Seasonal temperature and rainfall (value in brackets) correlation between WAPDA records (as in Table 1.2.1, 3-Khunjrab, 4-Ziarat, 5-Yasin, 6-Rama, 7-Ushkore, 8-Naltar, 9-Rattu). The values in bold italic style indicate statistically significant correlations (p=0.05). Upper triangle (June to September); lower triangle (December to April). All correlations are evaluated over the time period 1999-2008.

WAP	**3.**	**4.**	**5.**	**6.**	**7.**	**8.**	**9.**
3.		***0.80*** (-0.08)	***0.69*** (0.47)	***0.79*** (-0.12)	***0.73*** (-0.20)	***0.93*** (0.59)	***0.79*** (***0.65***)
4.	***0.76*** (0.16)		***0.66*** (0.23)	***0.65*** (0.49)	***0.85*** (-0.10)	***0.83*** (0.07)	0.58 (-0.19)
5.	***0.71*** (0.55)	0.56 (0.41)		***0.85*** (-0.27)	***0.89*** (0.24)	***0.85*** (0.43)	***0.78*** (0.50)
6.	***0.67*** (0.64)	0.40 (0.51)	***0.90*** (0.40)		***0.83*** (0.04)	***0.88*** (-0.07)	***0.96*** (-0.47)
7.	***0.75*** (0.40)	0.65 (***0.74***)	***0.92*** (0.34)	***0.74*** (0.34)		***0.86*** (-0.46)	***0.77*** (0.25)
8.	***0.69*** (0.59)	0.42 (0.49)	***0.82*** (***0.81***)	***0.76*** (***0.76***)	***0.86*** (0.33)		***0.85*** (-0.06)
9.	0.39 (0.10)	0.24 (-0.45)	***0.81***(-0.03)	***0.84*** (-0.15)	0.69 (-0.04)	0.54 (-0.06)	

Table 1.2.3b. As in Table 1.2.3a, but for PMD stations. The correlation is evaluated over the time period 1965-2000.

PMD	**Astore**	**Skardu**	**Gupis**	**Chitral**	**Gilgit**	**Bunji**	**Chilas**
Astore		***0.87 (0.79)***	***0.75 (0.58)***	***0.57 (0.11)***	***0.55 (0.07)***	***0.59 (0.04)***	***0.79 (0.02)***
Skardu	***0.97 (0.99)***		***0.97 (0.93)***	***0.85 (0.40)***	***0.76 (0.34)***	***0.63 (0.28)***	***0.74 (0.23)***
Gupis	***0.92 (0.94)***	***0.98 (0.96)***		***0.95 (0.52)***	***0.84 (0.45)***	***0.67 (0.38)***	***0.71 (0.31)***
Chitral	***0.91 (0.43)***	***0.92 (0.44)***	***0.95 (0.60)***		***0.93 (0.99)***	***0.76 (0.97)***	***0.70 (0.94)***
Gilgit	***0.84 (0.43)***	***0.81 (0.44)***	***0.84 (0.59)***	***0.97 (0.99)***		***0.93 (0.99)***	***0.85 (0.97)***
Bunji	***0.88 (0.43)***	***0.82 (0.44)***	***0.84 (0.59)***	***0.94 (0.99)***	***0.96 (0.99)***		***0.95 (0.99)***
Chilas	***0.87 (0.39)***	***0.78 (0.41)***	***0.79 (0.55)***	***0.85 (0.98)***	***0.85 (0.99)***	***0.96 (0.99)***	

Table 1.2.3a shows that in summer (above diagonal) the correlation between each pair of WAPDA temperature records is positive and, except for the pair Ziarat (4)-Rattu (9), significant. Also in winter (below diagonal) positive correlations occur, even though the number of pairs with statistically significant values becomes lower, while remaining larger than 50%. In general, temperature records exhibit better correlation over shorter than over longer distances, such as between the stations Rama (6)-Rattu (9) and Yasin (5)-Ushkore (7). The spatial correlation of precipitation shows a different behaviour. The correlation coefficients (shown under parenthesis) are generally lower, both during summer and winter, than for temperature, and they can be either positive or negative. The highest values (greater than 0.65) turn out to be the only ones that are also statistically significant and occur for the pair Khunjrab (3)-Rattu (9) in summer, and Ziarat (4)-Ushkore (7), Yasin (5)-Naltar (8), Rama (6)-Naltar (8) in winter. The spatial correlation between PMD station records, shown in Table 1.2.3b, are higher than those between the WAPDA stations, positive and statistically significant for each pair, for both precipitation and temperature. The correlation coefficients are generally larger for temperature than for precipitation.

The correlation coefficients of JJAS mean temperature inferred from the PMD station data are consistent with those found by Archer (2003), who calculated the correlation matrices between various weather stations in the UIB region, among which the Astore, Bunji, Gilgit and Skardu stations also employed here. Overall, rainfall correlations (shown in brackets) agree with the values reported in the paper by Archer and Fowler (2004), who analysed, among other station records, the Chitral, Gilgit, Bunji, Astore and Skardu station data. They found positive correlations between rainfall records from the various stations considered, but not all correlations turned out to be statistically significant from their analysis. It is worth pointing out, however, that, at variance with the present definition, Archer and Fowler (2004) referred to winter (summer) as the period including the months from October to March (April to September).

Our analysis highlights some differences in the temperature and precipitation spatial correlation as deduced from the analysis of PMD and WAPDA records. The maximum difference in altitude between the PMD stations employed in our study is about 1,100 m, while the altitude within the ensemble of WAPDA stations varies more, being the maximum difference of the order of 2,100 m (see Table 1.2.1). The WAPDA climate stations are all situated at higher altitudes than the PMD stations and, therefore, the analysed climatic variables (especially precipitation) could be more affected by elevation effects, leading to the less strong correlation between the WAPDA climate records than between the PMD climate records.

2.6 Temperature lapse rate and vertical precipitation gradients

Results for the seasonal vertical gradients of temperature and precipitation in northern Pakistan are shown in Fig. 1.2.4; each point in the plots represents the multiannual seasonal (JJAS and DJFMA) mean value of temperature (a,b) or precipitation (c,d) plotted against the altitude. Blue and red symbols indicate the Askole and Urdukas station data, respectively, while filled (empty) diamond symbols refer to the WAPDA (PMD) station data. The multiannual seasonal averages of precipitation and temperature were not calculated when the number of "good"-quality data was less than a predefined threshold (half the sample). This occurs for precipitation measurements at the Askole and Urdukas stations during winter, as shown in Fig. 1.2.4 c.

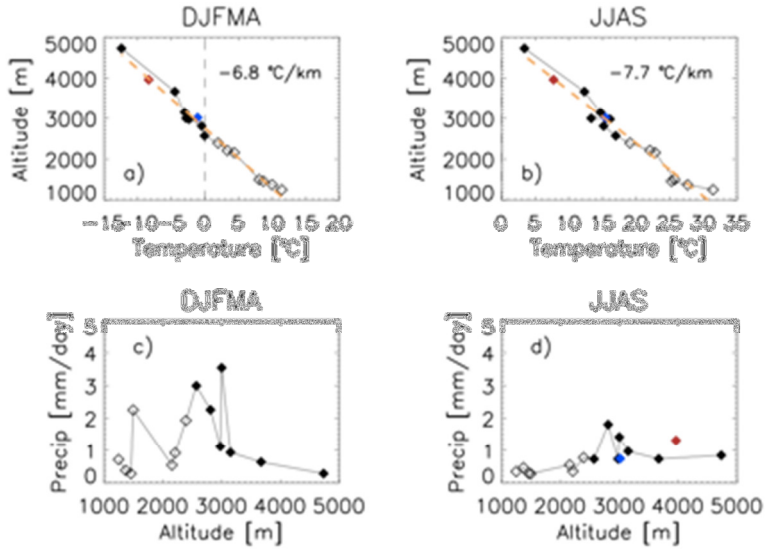

Figure 1.2.4. Winter (a,c) and summer (b,d) temperature (a,b) and precipitation (c,d) lapse rates derived from the measurements at the Askole (blue), Urdukas (red), PMD (empty diamond symbols), and WAPDA (filled symbols) stations.

The linear fit of the data gives a temperature lapse rate for the UIB region in winter (Fig. 1.2.4, panel a) and summer (panel b) of -6.8 °C 100 m^{-1} and -7.7 °C 100 m^{-1}, respectively. The winter value, in particular, is very close to the standard moist adiabatic lapse rate for the atmosphere (-6.5 °C 100 m^{-1}), as defined by the International Civil Aviation Organization (ICAO). This is consistent with the following statements: 1) in spite of the horizontal distance of stations and the presence of mountain barriers in, seasonal temperatures exhibit spatial coherence across the UIB region, and 2) one can expect that the high horizontal correlation between stations (as discussed above, significant for most station pairs) may be associated with the limited elevation differences.

The seasonal precipitation lapse rates shown in Figs. 1.2.4c and 1.2.4d seem to indicate that precipitation increases with altitude until about 3,000 m (well visible in summer), while it decreases from that altitude upwards. On the other hand, we expect an underestimation of precipitation measured at the highest elevations, due to the undercatch of solid precipitation by rain gauges. Winiger *et al*. (2005), using in-situ measurements of rain and snow, covering a profile from Gilgit to Khunjerab and including several sites in Yasin and Bagrot valleys, derived the vertical gradient of rainfall and snow water equivalent, showing that most differences between the two quantities arise above 3,500 m. At those levels, snow contribution can be as high as 80%-90% of total precipitation, while below usually rain dominates over snow (see figure 8 of the paper by Winiger *et al.*, 2005). It is interesting to observe that at an elevation of about 3,000 m, where our results suggest that a change in the precipitation vertical gradient occurs, solid and liquid precipitation are about equal according to the analyses performed by Winiger *et al.* (2005) and to the considerations drawn by Awan (2002). The presumable underestimation of high-altitude precipitation in summer (Fig. 1.2.4

d) seems also to indicate that, though much snowfall occurs in winter, summer snowfall contribution at high-elevation sites in this area is not negligible. According to previous studies, summer snowfall contribution at high-elevation sites is also much greater than for low-elevations sites (Hewitt, 2011). On the other hand, Fig. 1.2.4 (d) shows a slight increasing precipitation with altitude looking only at the two Ev-K2-CNR station data (Askole, 3,015 m a.s.l., and Urdukas, 3,962 m a.s.l.). It also shows that the averaged JJAS precipitation at Urdukas is higher than that at the closest (in terms of altitude) WAPDA stations, i.e., Khunjerab (4,710 m a.s.l.) and Ziarat (3,669 m a.s.l.). This might be attributable to the minimum effect of the monsoon to the north of the region, where Khunjerab and Ziarat are located, because the Karakoram mountains generally limit the occasional intrusion of monsoon air masses.

The paper "Climatic characterization of the Baltoro glacier area and northern Pakistan from in-situ stations" by Palazzi et al. is in preparation for the International Journal of Climatology.

3. Winter precipitation in the Karakoram and western weather patterns

We have investigated the properties of the synoptic-scale circulation affecting the mountain regions of northern Pakistan, by analysing 6-days-long back trajectories with the Hybrid Single Particle Lagrangian Integrated Trajectory (HYSPLIT) Model (http://ready.arl.noaa.gov/HYSPLIT.php, Draxler and Hess, 1998). Trajectory calculations are based on the operational Global Data Assimilation System (GDAS) produced by the United States National Centres for Environmental Prediction (NCEP) with a horizontal resolution of 1°x1°. HYSPLIT back-trajectory ensembles, providing the geographic location and altitude of air parcels with 1-hour resolution along each path, have been calculated for two sets of five different receptor points centred at 35.73°N-76.29°E and shifted by ± 0.75°, respectively at 100 m and 500 m above ground level (a.g.l), representative of the mountain area of northern Pakistan. The runs were performed for the years 2005-2009, more or less covering the time period of measurements at the Askole and Urdukas stations we have analysed (see Sect. 2), separately for summer (JJAS) and winter (DJFMA) seasons. This allowed obtaining a database of three-dimensional back-trajectories for the focus area firstly providing an insight, by means of "descriptive" maps, of the air-mass flows towards the northern Pakistan mountain area in the two seasons. Panels a and b of Fig. 1.3.1 show the air-mass back trajectories reaching northern Pakistan during summer and winter, respectively.

To better emphasize the transport paths also on "peripheral" regions far away from the two measurement sites in the Baltoro, a logarithmic scale is adopted for the number of back-trajectories in Fig. 1.3.1. The region of northern Pakistan is predominantly prone to a westerly synoptic-scale circulation, in agreement with several studies illustrating the role of western disturbances affecting the Karakoram and western Himalaya precipitation (e.g., Treydte *et al.*, 2006; Syed et al., 2006). To better understand the impact on precipitation of synoptic-scale circulations, panels c and d show only those air-mass trajectories actually associated with precipitation events occurred on the target area, based on the inspection of the Urdukas and Askole precipitation data in the period 2004-2009.

Panel d of Fig. 1.3.1 clearly shows that precipitation in winter over the target area is carried on westerly air masses, with sporadic contributions from the latitudes above 40°N. In contrast to central and southern Pakistan (PMD, 2009), northern Pakistan appears not to be strongly affected by the monsoon activity during summer (panel c) and only a few instances of air transport from the Indian Ocean are detected in the back-trajectory analyses. They are usually associated with the migration on monsoonal depressions from the Arabian sea and the Bay of Bengal, also related to the summertime position of the Inter-Tropical Convergence

Zone (ITCZ) located over southern Pakistan, probably due to the summertime migration of the ICTZ northward.

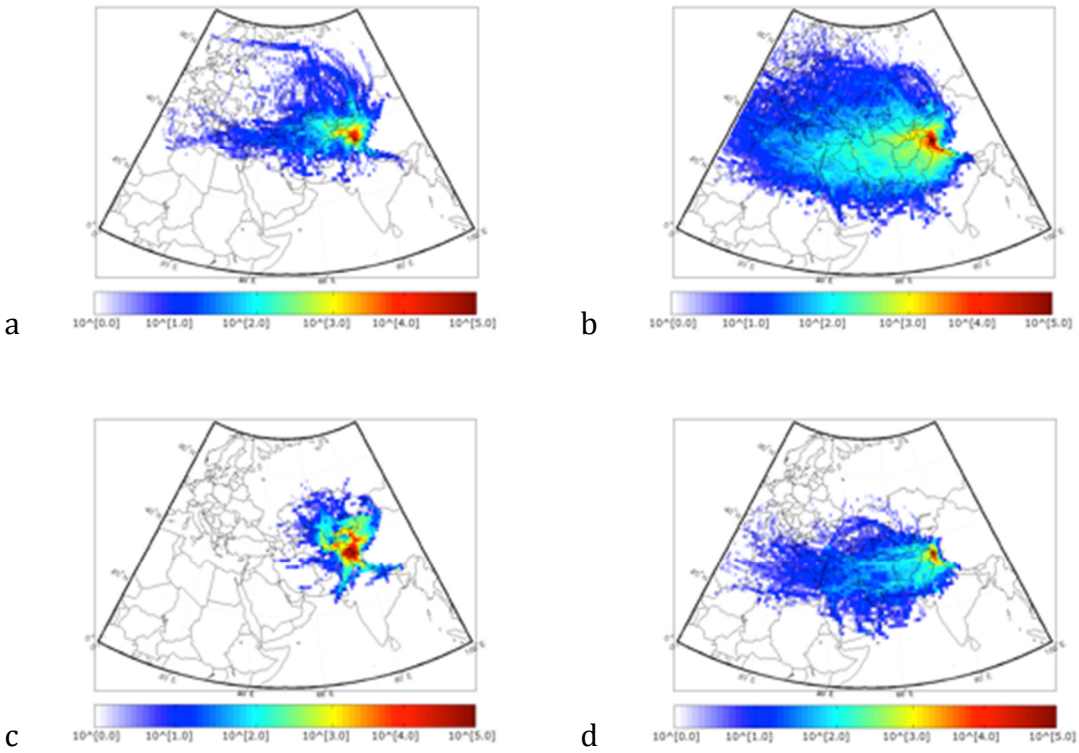

Figure 1.3.1. Air-mass back-trajectories describing the synoptic-scale atmospheric circulation in northern Pakistan. The coloured logarithmic scale indicates the number of back-trajectory points for summer (left column plots) and for winter (right column plots). a,b) back-trajectory ensembles for all events; c,d) back-trajectory ensembles associated to precipitation events over the target area.

As already mentioned, western weather patterns originate in the Atlantic and the Mediterranean, they move eastward and bring moisture and precipitation over the HKK region. To give an idea of the trajectories followed by these disturbances, Fig. 1.3.2 shows the precipitation during three different winters obtained from satellite TRMM daily data, plotted as a function of the longitude (x-axis) and time (November to March, y-axis). The displayed longitudes, from 30°E to 80°E, include a region from the eastern Mediterranean to the HKK. Precipitation is averaged over the latitude band from 30°N to 40°N. The westerly disturbances appear as non-homogeneous rainy systems. Their intensification east of about 40°E could suggest that an input of extra moisture from other sources than Mediterranean, i.e., the Caspian and Arabian Sea and the Persian Gulf, could be of importance. The picture obtained from TRMM data is consistent with the one obtained from ERA40 reanalyses and EC-Earth model data, not shown here.

4. Conclusions

We have analyzed the properties of precipitation in mountain areas located above 1,000 m above mean sea level in the HKK and Himalayan regions, focusing on precipitation patterns, seasonality and trends as revealed by various existing gridded precipitation datasets, including a satellite dataset (the TRMM 3B42 product), raingauge based collections (APRHODITE, CRU, GPCC), a merged satellite-raingauge climatology (GPCP), a reanalysis product (ERA-Interim) and precipitation data from a state-of-the-art Global Climate Model (EC-Earth).

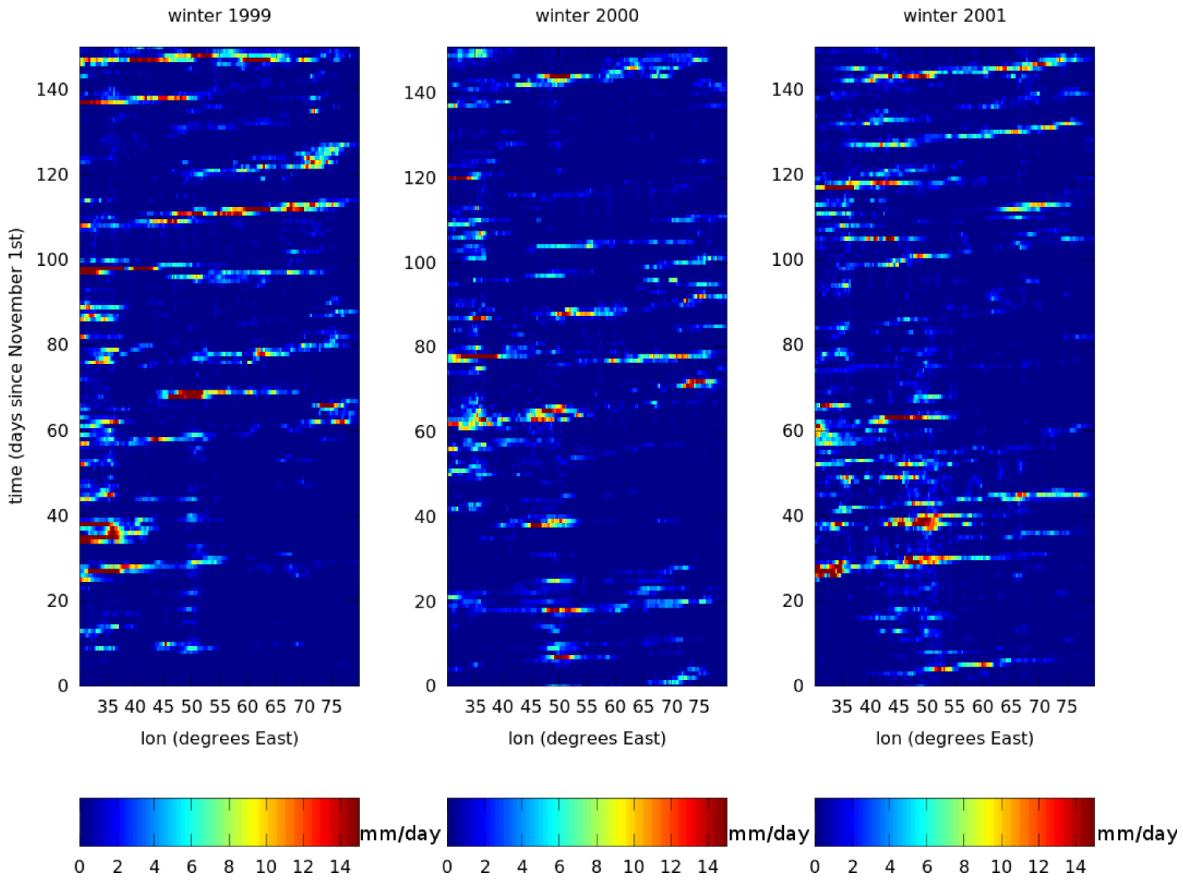

Figure 1.3.2. TRMM daily precipitation averaged over latitudes from 30°N to 40°N, plotted as a function of longitude (from 30°E to 80°E) and time for winters (NDJFM) 1999, 2000 and 2001 (left to right).

All the currently available gridded observational datasets are perforce limited to coarse resolutions. This makes them suitable for large-scale global studies, and for applications such as the comparison and validation of climate models at global scales or the comparison with global reanalysis products. Though their application to assess the climate in smaller and orographically complex regions, such as the HKKH, is more difficult owing to their limited resolution, and the limited coverage and inhomogeneity in the spatial and altitudinal distribution of the measuring sites, our analysis shows that it is anyway possible to obtain a consistent picture of climate at the seasonal scale from these datasets in terms of area-averages over sub-regions of the HKKH. On the other hand, there are severe difficulties in considering any of these observational/reanalysis datasets as a reference or ground truth for precipitation, and thus multi-probe source data should always be considered for estimating the hydrological cycle in these areas.

The mean annual cycle of precipitation over HKK and Himalaya is coherently reproduced by the various datasets. In the HKK it is characterized by a bimodal precipitation distribution, reflecting the wintertime precipitation associated with the western weather patterns and the impact of the summer monsoon. In the Himalaya, the dominant source of precipitation is the summer monsoon, leading to a unimodal precipitation distribution peaked around July.

The precipitation time series from the various datasets in the time period 1950-2010 reproduce, in spite of the biases between the datasets, the inter-annual precipitation variability in a coherent way. None of the datasets shows statistically significant trends in the HKK during winter. In the Himalaya during summer, a statistically significant decreasing trend is observed from the analysis of the longest datasets (APHRODITE, CRU and GPCC). Outputs from EC-Earth indicate a positive summer precipitation trend in this region, opposite

to what is revealed by the observations: a possible explanation for the discrepancy between the decreasing trend in the observations and the increasing monsoon precipitation predicted by EC-Earth is that the model does not correctly reproduce the complex effect of the recent increase of atmospheric aerosols resulting from the combustion of fossil fuels in Asia (Ramanathan et al., 2005; Lau et al., 2006; Bollasina et al., 2011).

Projections made with EC-Earth under two different emission scenarios, RCP 4.5 and RCP 8.5, show for RCP 4.5 that the historical increasing precipitation trend in the Himalaya during summer is predicted to continue until about 2050, starting a slight decrease from that time on. In the RCP 8.5 scenario, summer precipitation is found to increase throughout the century, associated with an increasing trend in the intensity of rainfall events, a slight reduction of the number of rainy days. In this scenario, the hydroclimatic intensity index is also found to increase, indicating a transition towards more episodic and intense monsoonal precipitation. Overall, these results agree with most current climate model projections (Solomon et al., 2007) giving an increase in wet extremes, in the length of dry periods and in precipitation in the Indian monsoon by the end of the 21st century, as a result of atmospheric moisture build-up due to increased greenhouse gases and consequent temperature increase. Future projections in the HKKH region should be further verified with climate models interactively resolving temporally varying radiative and thermodynamical effects of various aerosol species.

High-resolution in-situ measurements of climatic variables in mountainous regions are still quite rare, though substantial progress has been made in the last decades in expanding the station coverage over mountains using automatic weather stations. Precipitation is probably the most critical variable to be measured, owing to the technical difficulty of measuring snowfall contribution accurately (Winiger at al. 2005; Rasmussen et al. 2012). The number and density of measuring stations in mountainous regions is typically much higher in the valley floors than in the most active hydrological zones. Though this is also the situation encountered in the Karakoram range, the number of research programmes focused on this region has recently increased.

In this study, we have analysed the results of the meteorological measurements carried out during the first five years of operation of two automatic weather stations installed at Askole (3,015 m a.s.l.) and Urdukas (3,962 m a.s.l.) on the Baltoro glacier, part of the Karakoram range in northern Pakistan, in the framework of the SHARE programme of the Italian National Research Council and Ev-K2-CNR committee. The data collected at the Askole and Urdukas stations have been analyzed to characterize the meteoclimatic conditions in the proximity of the Baltoro glacier. We have complemented this analysis with temperature and precipitation data measured at fourteen other climatic stations spread over northern Pakistan, managed by the PMD and WAPDA agencies, providing longer records than those provided so far by the two stations in the Baltoro.

It is quite clear, as confirmed by the analysis presented in Sect. 2 using the PMD data, that the mountainous regions of northern Pakistan have experienced “anomalous” cooling trends since the 1960s during summer, compared to other elevated regions of the world which have warmed (e.g., Liu *et al.* 2009, Qin *et al.* 2009 and Rangwala *et al*. 2009, Lu *et al*., 2010) and in particular to the neighbouring Himalayan mountains. However, though in line with the other studies, our results for seasonal trends (especially for precipitation tendencies) suggest that the ability to interpret these results conclusively is still limited, probably by the unevenness and paucity of adequate observations at different elevations and by the specificity of the climatic responses in different parts of this region.

In this study, we have used PMD and WAPDA data to assess the extent to which the single stations located at different altitudes may be considered as representative of the area in which they are located, through the calculation of the regional correlation between the

temperature and precipitation records measured at the various locations. Assessing the regional correlation of temperature and precipitation is important in view of better understanding the temperature and precipitation dependence on the elevation in these areas. Temperature is spatially highly correlated across the UIB region, in summer and winter, at typically valley altitudes (below about 2,400 m a.s.l), as well as at higher elevations (from ~2,400 to 4,700 m a.s.l.). Precipitation is spatially less correlated, in particular in the higher altitude regions where the orographic effect, major source of uncertainty in precipitation estimates, plays an important role. As a consequence, while the average temperature lapse rate in the UIB, inferred from all station data, is consistent with the moist adiabatic lapse rate of the atmosphere, the expected dependence of precipitation on the elevation (increasing precipitation with increasing altitude) does not emerge from our analysis. Precipitation is observed to increase until about 3,000 m and to decrease thereafter.

Large-scale synoptic circulations play a fundamental role to explain the observed climatic responses of the HKK area. We have made use of back-trajectory ensembles calculated for a receptor point representative of the mountain area of northern Pakistan to link local conditions to synoptic-scale conditions. Our analysis shows that the Karakoram area is not dominated by a monsoon-controlled dynamics as the eastern Himalaya and other South-Asian regions, but it is mainly influenced by westerly disturbances during winter and spring. Western weather systems originate in the north-eastern Atlantic and in the Mediterranean and bring moisture and precipitation over the Central-Southwest Asia.

The next months will be dedicated to the investigation of the mechanisms associated with western weather patterns, their strengthening as they encounter a region of enhanced low pressure and their enrichment in terms of moisture from source areas such as the Caspian sea. Due to the origin area of these disturbances, the North Atlantic Oscillation (NAO) is expected to play an important role in influencing the western weather patterns activity and, by consequence, winter precipitation in the Karakoram. Therefore, our next activities will be particularly focused on the investigation of the link between the NAO and 1) evaporation/relative humidity patterns in the area extending from the Atlantic to the Karakoram and 2) precipitation in the Karakoram area.

References

Archer DR. 2003. Contrasting hydrological regimes in the upper Indus Basin. Journal of Hydrology 274 (1-4): 198-210.

Archer, D. R., and H. J. Fowler (2004), Spatial and temporal variations in precipitation in the upper Indus basin, global teleconnections and hydrological implications, Hydrol. Earth Syst. Sci., 8, 47–61, doi:10.5194/hess-8-47-2004.

Awan SA. 2002. The Climate and Flood Northern Areas of Pakistan, Risk Potential of Commission on Science and Technology for Sustainable Development in the South. (http://www.sciencevision.org.pk/BackIssues/Vol7/Vol7No34/Vol7No3&4_10_Climate_Flood_ShaukatAwan.pdf).

Barros, A. P., M. Joshi, J. Putkonen, and D. W. Burbank (2000), A study of the 1999 mon- soon rainfall in a mountainous region in central Nepal using TRMM products and rain gauge observations, Geophys. Res. Lett., 27, 3683–3686, doi:10.1029/2000GL011827.

Bollasina, M. A., Y. Ming, and V. Ramaswamy (2011), Anthropogenic Aerosols and the weakening of the south Asian summer monsoon, Science, 334(6055), 502–505, doi: 10.1126/science.1204994.

Bookhagen, B., and D. Burbank (2006), Topography, relief, and TRMM-derived rainfall varia- tions along the Himalaya, Geophys. Res. Lett., 33, L08405, doi:10.1029/2006GL026037

Bookhagen, B., and D. Burbank (2010), Toward a complete Himalayan hydrological budget: Spatiotemporal distribution of snowmelt and rainfall and their impact on river discharge, J. Geophys. Res., 115, F03019, doi:10.1029/2009JF001426.

Draxler RR, Hess GD. 1998. An overview of the HYSPLIT_4 modeling system of trajectories, dispersion, and deposition. Australian Meteorological Magazine 47: 295-308.

Dutra, E., G. Balsamo, P. Viterbo, P. M. A. Miranda, A. Beljaars, C. Schaïr, and K. Elder (2010), An improved snow scheme for the ECMWF land surface model: Description and offline validation, J. Hydrometeor., 11(4), 899–916, doi:10.1175/2010JHM1249.1.

Fowler HJ, Archer DR. 2006. Conflicting Signals of Climatic Change in the Upper Indus Basin. Journal of Climate 19: 4276-4293. DOI: http://dx.doi.org/10.1175/JCLI3860.1

Giorgi, F., E.-S. Im, E. Coppola, N. S. Diffenbaugh, X. J. Gao, L. Mariotti, and Y. Shi (2011), Higher hydroclimatic intensity with global warming, J. Climate, 24, 5309–5324, doi: 10.1175/2011JCLI3979.1.

Hazeleger, W., et al. (2012), EC-Earth v2.2: description and validation of a new seamless earth system prediction model, Clim. Dynam., pp. 1–19, doi:10.1007/s00382-011-1228-5.

Hewitt K. 2011. Glacier Change, Concentration, and Elevation Effects in the Karakoram Himalaya, Upper Indus Basin, Mountain Research and Development 31 (3): 188-200.

Lau, K., M. Kim, and K. Kim (2006), Asian monsoon anomalies induced by aerosol direct forcing, Clim. Dynam., 26, 855–864, doi:10.1007/s00382-006-0114-z.

Liu X, Cheng Z, Yan L, Yin Z. 2009. Elevation dependency of recent and future minimum surface air temperature trends in the Tibetan Plateau and its surroundings. Global and Planetary Change 68: 164-174.

Lu A, Kang S, Li Z, Theakstone W. 2010. Altitude effects of climatic variation on Tibetan Plateau and its vicinities. Journal of Earth Science 21: 189-198.

Moss, R. H., et al. (2010), The next generation of scenarios for climate change research and assessment, Nature, 463(7282), 747–756, doi:10.1038/nature08823.

Palazzi E., von Hardenberg J. and Provenzale A. (2013) Precipitation in the Hindu-Kush Karakoram Himalaya: Observations and future scenarios, Journal of Geophysical Research: Atmospheres doi: 10.1029/2012JD018697.

PMD. 2009. Pakistan Meteorological Department, Technical Report No. PMD-22/2009.

Qin J, Yang K, Liang S, Guo X. 2009. The altitudinal dependence of recent rapid warming over the Tibetan Plateau. Climatic Change 97: 321-327.

Ramanathan, V., et al. (2005), Atmospheric brown clouds: Impacts on south Asian climate and

hydrological cycle, Proc. Natl. Acad. Sci., 102, 5326–5333, doi:10.1073/pnas.0500656102.

Rangwala I, Miller J, Xu M. 2009. Warming in the Tibetan Plateau: possible influences of the changes in surface water vapor. Geophysical Research Letters 36: L06703.

Rasmussen, R., et al. (2012), How well are we measuring snow?, BAMS, June 2012, 811–829, doi:http://dx.doi.org/10.1175/BAMS-D-11-00052.1

Solomon, S., D. Qin, M. Manning, M. Marquis, K. Averyt, M. M. B. Tignor, H. L. M. Jr., and E. Z. Chen (2007), Climate Change 2007: The physical science basis. contribution of working group I to the fourth assessment report of the Intergovernmental Panel on Climate Change.

Syed FS, Giorgi F, Pal JS, King MP. 2006. Effect of remote forcings on the winter precipitation of central southwest Asia part 1: observations. Theoretical and Applied Climatology 86: 147-160

Treydte KS, Schleser GH, Helle G, Frank DC, Winiger M, Haug GH, Esper J. 2006. The twentieth century was the wettest period in northern Pakistan over the past millennium. Nature 440: 1179-1182. DOI: 10.1038/nature04743.

Winiger M, Gumpert M, Yamout H. 2005. Karakorum-Hindukush-western Himalaya: assessing high altitude water resources. Hydrological Processes 19: 2329-2338.

World Meteorological Organization, 2008. Guide to Meteorological Instruments and Methods of Observation, WMO No. 8.

Young GJ, Hewitt K. (1990). Hydrology research in the Upper Indus Basin, Karakoram Himalaya, Pakistan. Hydrology of Mountanous Areas, Czechoslovakia, 139-152.

Zahumenský I. 2004. Guidelines on Quality Control Procedures for Data from Automatic Weather Stations, CBS/OPAG-IOS/ET AWS-3/Doc. 4(1), (25.V.2004), World Meteorological Organization.

Project of Strategic Interest NEXTDATA

D2.6.b - Results of the pilot study:
"Analysis of terrestrial biodiversity and ecosystem changes in high-elevation regions"

Prepared by: Ramona Viterbi (Gran Paradiso National Park)

Contributors:
Cristiana Cerrato (CNR-ISAC), Antonello Provenzale (CNR-ISAC)

Main Objectives

The main objective of this pilot study is the assessment of changes in biodiversity and ecosystems in high-altitude mountain areas, by statistical analysis and interpretation of the data collected and to be collected during the project.

In particular, this pilot study aims at improving data monitoring and storage methodologies, in order to explore the relationships between animal biodiversity, climate and land use at different spatial scales in alpine protected areas. The long-term purpose is to create the baseline – through the conduction of a monitoring program to be repeated every 5 years - against which to evaluate future changes.

The study is characterised by 2 different steps:

- the conduction of a new monitoring campaign;
- the identification, collection and analysis of previous data on terrestrial biodiversity in the western Italian Alps.

1. The new monitoring campaign (April-December 2012)

Research activities have been carried out in specific sites, already monitored during the years 2007-2008. These activities represent the implementation of a previous project, promoted by the Gran Paradiso National Park in 2006 and continued with the cooperation between CNR-ISAC and other two protected National Park areas in NW Italian Alps, the Orsiera Rocciavré Natural Park and Veglia Devero Natural Park.

The first aims of the research are to create a historical dataset containing the existing data and to improve some of the methodologies applied to the monitoring of animal biodiversity.

The 2012 monitoring activities have been carried out in the three Parks mentioned above (Gran Paradiso National Park, Orsiera-Rocciavré Natural Park, Veglia Devero Natural Park). Thirteen altitudinal transects chosen between 500 to 2700 m a.s.l. were set, each covering an altitudinal range of 1000 meters; three vegetation belts (montane, subalpine, alpine) were thus included.

Sampling units are circular plots (100 m radius), for a total of 75 sampling stations, where monitoring activities have been carried out to provide presence/absence and data on the relative abundance of species belonging to taxa, selected as bio-indicators.

Selected taxa are: Lepidoptera Rhopalocera (butterflies), Orthoptera (grasshoppers/ crickets), birds, surface-active macro-arthropods (Coleoptera Carabidae, Coleoptera Staphylinidae, Araneae, Formicidae).

For each taxonomic group we used semi-quantitative census techniques; the latter were generally quite easy to apply, standardized, cheap and repeatable. The bird census was performed by means of point counts and each plot was visited twice during the reproductive season. We sampled butterflies and grasshoppers/crickets using walking transects along the diameter of the plot (200 m in length), walked at uniform speed. We collected surface-active arthropods using pitfall traps (plastic cups, diameter of 7 cm, filled with 10 cc of white vinegar).

All field activities were conducted from mid April to mid October 2012.

After field work (October - December 2012), we started the laboratory analysis of collected samples. As for butterflies and grasshoppers/crickets, we started the identification of collected specimens and the preparation of a reference collection. As for the selected groups of surface-active macro-arthropods (Coleoptera Carabidae, Coleoptera Staphylinidae, Araneae, Formicidae), we started the identification at the morpho-species level. All specimens were stored and preserved in alcohol 70%. Expert taxonomists will make further analyses to identify the samples at species level.

As a result of the monitoring activities, we have produced databases, consisting of the lists of species and their relative abundance, for each taxon and each sampling plot. So far, only the database of birds has been completed. For the other taxa, the identification of collected specimens is not yet completed (butterflies, grasshoppers/crickets, surface active macro-arthropods).

During laboratory activities, we also experimented a working protocol for the measurement of arthropod biomass (surface-active macro-arthropods), both in terms of weight and volume.

Monitoring activities concerned also the collection of:

- micro-climatic data, through the positioning of temperature data-loggers (iButton DS1922), one per each sampling station and for the whole sampling season;
- macro-environmental (topographic variables) and micro-environmental parameters (percentage of land coverage and estimate of floristic diversity).

These data are now stored in appropriate databases.

2. Identification, collection and analysis of previous data on terrestrial biodiversity in the western Italian Alps

2.1 Description of biodiversity patterns

We have performed a statistical analysis of 2007-2008 campaign data, in order to assess the pattern of congruence or diversity in the distribution of five taxonomic groups along altitudinal gradients and to determine the relative role of geographical, environmental and climatic factors. We present in the following the results for species richness and community composition, showing how arthropods are highly influenced by micro-climate and are potentially vulnerable to changes in temperature.

Species richness

Our results suggest that, for the altitudinal gradient which we have explored, the curve of the overall species richness is hump-shaped, with a peak in richness at intermediate elevations and a stronger decline at increasing elevations (Fig. 2.2.1a). Similar patterns have been observed in other studies for various taxonomic groups, e.g. vascular plants (Grytnes 2003), ferns (Bhattarai et al. 2004), insects (Fleishman et al. 1998), birds (Kessler et al. 2001) and small mammals (Rickart 2001, Sanchez-Cordero 2001). Percentages of vulnerable and endemic species were related ($\rho = 0.568$, $N = 69$, $p < 0.0001$); both quantities are found to increase in a monotonic way along the altitudinal gradient (Fig. 2.2.1b).

As observed in other studies (e.g., Oommen and Shanker 2005), we found that temperature was the most important variable in determining species richness associated with altitude (Table 2.2.1). This held for almost all taxonomic groups and for the overall species richness. Only butterflies and carabids showed a slightly different pattern, as they were more influenced by environmental variables

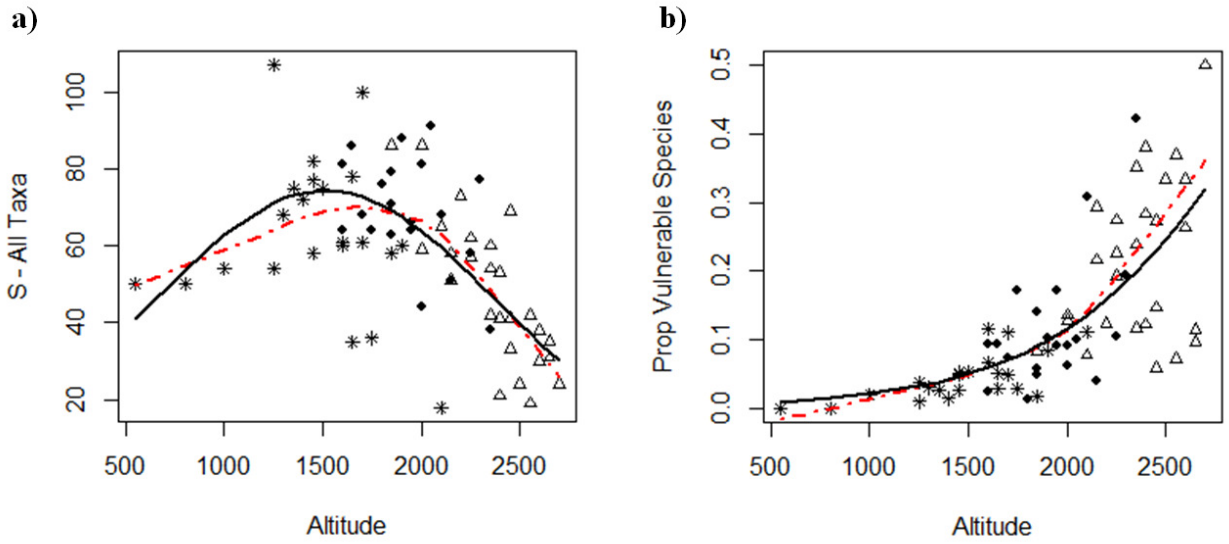

Figure 2.2.1. Scatterplots of the total species richness per site for all taxa pooled together (a) and of the proportion of vulnerable species (b) along the altitudinal gradient. The LOWESS regression curve is represented as a dashed line, while the significant regression curve is represented as a solid line. Montane belt (*), Subalpine belt (●), Alpine belt (△).

Temperature showed a quadratic relationship for all taxa pooled together and for the individual taxonomic groups, with a peak at intermediate temperatures. Only the proportion of endemic species clearly decreased along the temperature gradient, while the proportion of vulnerable species decreased with temperature, but increased at the second extreme of the gradient, as described by a quadratic function with a positive coefficient of the second order term.

We found the highest levels of species richness in the Subalpine belt, as could be expected from the fact that this is a transition area where different habitats coexist (Lomolino 2001, Oommen and Shanker 2005). On the contrary, the Alpine belt presents lower values of species richness, but a higher percentage of species of conservation concern (e.g., microtherm species, highly specialized species with low dispersal capability, rare species - Fig. 2.2.2).

Endemic and vulnerable species often present very narrow ranges and their abundance peaks are not necessarily coherent with species richness, being often shifted to higher altitudes

(Kessler 2002, Vetaas and Grytnes 2002, Fu et al. 2006, Schmitt 2009). In addition, the Alpine belt is characterized by environmental constraints (severe climatic conditions, short summer periods, slope, natural hazards) and by the importance of direct and indirect effects of climatological factors, in particular low temperatures (Beniston 2003, Pauli et al. 2004, Körner et al. 2011).

Table 2.2.1. Results of variation partitioning for all taxa pooled together, for each taxonomic group and for the percentage of vulnerable and endemic species. Mod represents the single variables selected for each group, after forward selection procedures and linear regression models. Variations in species composition are explained by four group of variables: altitude (Alt), temperature (Temp), vegetation (Veg), geography (UTM); Unex represents the unexplained variance; Exp the total variance explained by each group of variable and Pure the unique effect of each group. The sign of interaction is represented in brackets. Significance values of each fraction have been calculated by using 999 random permutations. ° p < 0.10; * p < 0.05; ** p < 0.01; *** p < 0.01
Code for variables are the following: altitude (Alt), temperature (Temp), structural diversity (Str Div), trees (Tree), tall shrubs (TShr), low shrubs (LShr), herbaceous layer (HerbL), stone (Rock), UTM longitude (x), UTM latitude (y).

		Carabids	Butterflies	Spiders	Staphylinids	Birds	Endemic	Vulnerable
Alt	Mod	NA	(-) Alt	(-) Alt, (-) Alt^2	(-) Alt, (-) Alt^2	(-) Alt, (-) Alt^2	(+) Alt	(+) Alt
	Exp	NA	9.7*	23.6***	42.0***	35.0***	32.3***	44.6***
	Pure	NA	1.9^{ns}	1.5^{ns}	9.6*	0^{ns}	0^{ns}	0^{ns}
Temp	Mod	NA	(+) Temp, (-) Temp^2	(+) Temp, (-) Temp^2	(-) Temp, (-) Temp^2	(+) Temp, (-) Temp^2	(-) Temp	(-) Temp, (+) Temp2
	Exp	NA	23.5***	20.9**	30.6***	37.5***	31.9***	64.7***
	Pure	NA	8.7*	0^{ns}	0^{ns}	0.5^{ns}	0^{ns}	4.9°
Veg	Mod	(+) HerbL	(+) Str Div, (+) HerbL	(-) Rock	(-) Rock, (+) Tree	(-) Rock, (+) Str Div	(+) Rock, (-) Str Div	(+) Rock, (-) Tree, (-) TShr
	Exp	12.1**	30.1***	13.3**	26.8***	32.4***	23.5***	36.8***
	Pure	12.1**	11.7*	1.0^{ns}	1.0^{ns}	3.8^{ns}	6°	0^{ns}
UTM	Mod	NA	NA	NA	NA	NA	NA	(+) x
	Exp	NA	NA	NA	NA	NA	NA	20.5***
	Pure	NA	NA	NA	NA	NA	NA	6*
Unex		87.85	60.71	77.1	57.74	58.66	62.07	70.07

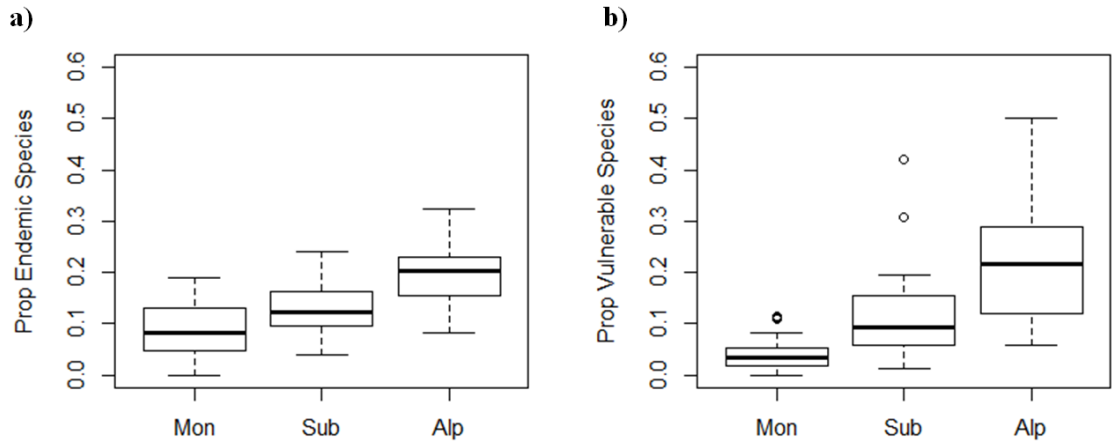

Figure 2.2.2. Percentage of species of conservation concern, endemic (a) and vulnerable (b) species, in the different belts. The boxes show median, first and third quartile, whiskers represent minimum and maximum values and outliers are plotted as circles. Montane belt (Mon), Subalpine belt (Sub), Alpine belt (Alp).

Community composition

The analysis of community composition showed the presence of a less clear pattern: this is confirmed by all three approaches that we adopted in analysing the species-per-site matrices.

The site ordination for all taxa, as obtained by Correspondence Analysis (CA) is shown in Fig.

2.2.3a. Percentage of inertia explained by the first axis ranged between 6.914 for spiders to 13.882 for birds and was 7.499 in the case of all taxa pooled together.

The low percentage of inertia explained by the first two axes of the Correspondence Analysis (CA) indicated that the pattern of community composition was more complex and cannot be easily summarized in a space with reduced dimensionality. Species distribution along the first CA axis displayed a smooth transition, leading to a large separation at the extremes of the gradients (Brehm et al. 2003). Different belts showed no clear-cut separation, but led to very different community composition (Fig. 2.2.3b).

Spearman rank correlation between scores along the first CA axis and environmental variables indicated that the compositional gradients were mainly correlated with altitude and temperature (Table 2.2.2).

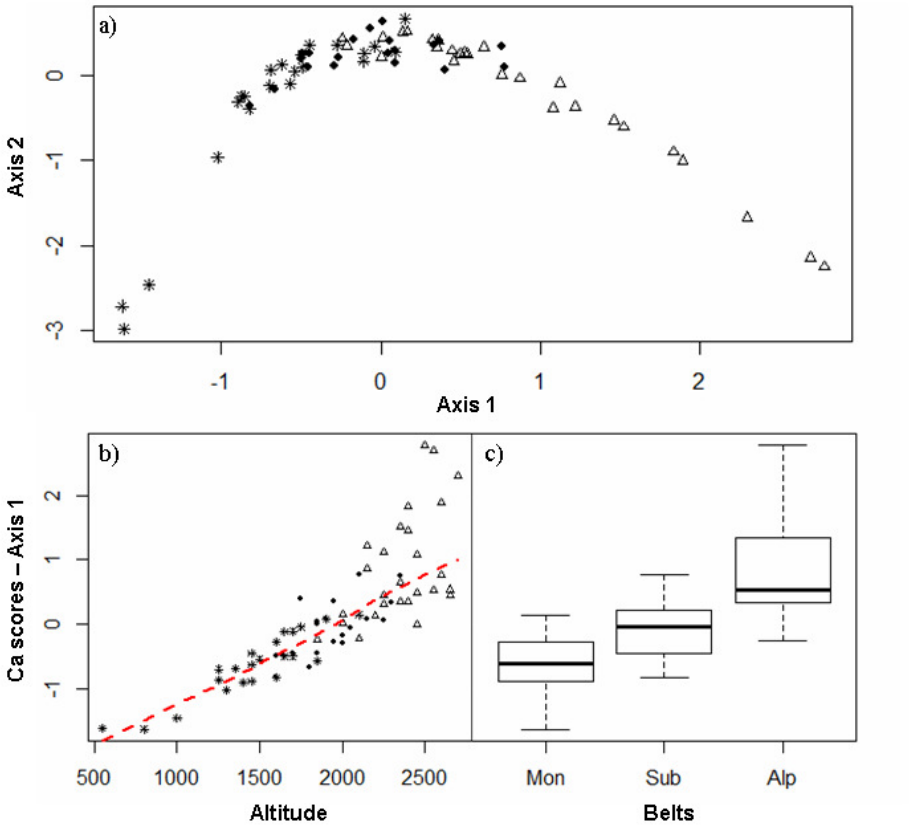

Figure 2.2.3. a) Correspondence Analysis (CA) for the 69 sampling sites, based on data from all taxa pooled together. Montane belt (*), Subalpine belt (●), Alpine belt (△). b). Scatterplot between site scores along the first axis of the CA with all taxa pooled together and altitude. The LOWESS regression is represented as a dashed line. c) Box-plot of site scores among vegetation belts. Montane belt (Mon), Subalpine belt (Sub), Alpine belt (Alp).

The analysis of variation partitioning applied to a CCA showed that all the fractions explained only low amount of variation suggesting a highly complex succession of species along the ecological gradients under study. Moreover, the temperature effect is highly shared with altitude, but presented a pure effect which is larger than altitude, in all cases except for birds (Fig. 2.2.4).

Results from the distance-based approach (the Mantel test) confirmed these considerations. We observed, in almost all taxonomic groups, an influence of altitude and temperature on differences in community composition. Partialling out the effect of temperature, altitude lost significance for all taxonomic groups except birds. On the contrary, when the effect of altitude was removed first, temperature still remained important, even though caution should be

adopted when interpreting the results from partial Mantel tests (Raufaste and Rousset 2001) (Table 2.2.3).

Table 2.2.2. Spearman correlation coefficient between each environmental variable and the extracted scores of the first dimension of Correspondence Analysis (CA) for the five taxa and all taxa pooled together. ScoreAx1 = scores of the sampling sites along the first CA dimension. * $p < 0.05$; ** $p < 0.01$, after sequential Bonferroni procedure. For abbreviations see Table 2.2.1.

	Alt	Temp	StrDiv	Tree%	TShr%	LShr%	HerL%	Rock%	x	y
ScoreAx1$_{car}$	0.581**	-0.624**	-0.396*	-0.321	-0.424**	-0.264	0.085	0.033	0.607**	0.774**
ScoreAx1$_{but}$	-0.863**	0.883**	0.487**	0.606**	0.619**	0.197	-0.248	-0.03	-0.381*	-0.477**
ScoreAx1$_{spi}$	-0.821**	0.850**	0.398*	0.490**	0.580**	0.170	-0.134	-0.135	-0.325	-0.461**
ScoreAx1$_{sta}$	-0.516**	0.618**	0.089	0.227	0.188	-0.086	0.205	-0.077	-0.215	-0.310
ScoreAx1$_{bir}$	0.912**	-0.852**	-0.589**	-0.788**	-0.678**	-0.371*	0.377*	0.219	0.226	0.257
ScoreAx1$_{all}$	0.891**	-0.919**	-0.470**	-0.560**	-0.600**	-0.214	0.188	0.128	0.346	0.481**

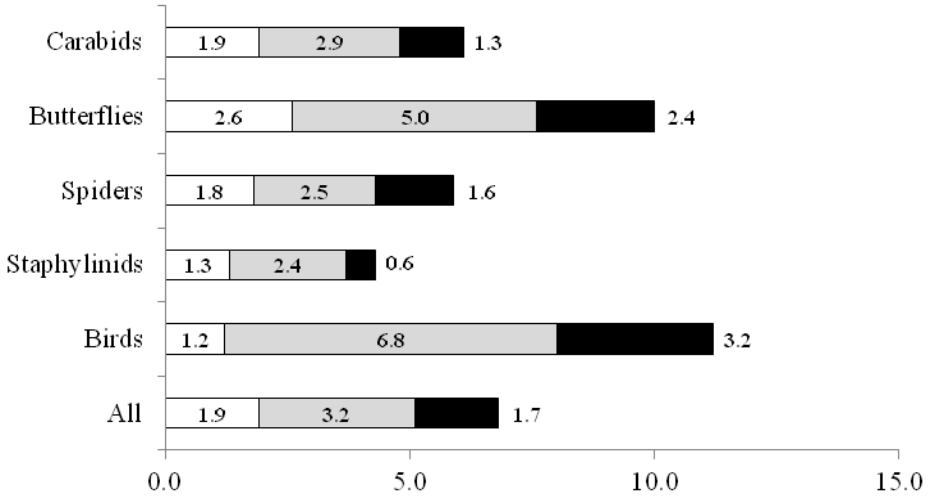

Figure 2.2.4. Variation partitioning for CCA. The pure effects of temperature (white) and altitude (black) and their shared effect (grey) are represented.

All these results indicate that temperature differences affected the community composition of the invertebrates studied here, in keeping with the fact that poikolothermic and ectothermic organisms are particularly sensitive to climate (Huey and Stevenson 1979, Hodkinson 2005). For all invertebrate groups, the role of geographic distance in shaping community composition remained significant, even when controlling for the other factors. These results indicate that, in terms of invertebrate communities, each protected area presents peculiarities that cannot be explained by factors other than geographical characteristics and distance from each other.

Conclusions

When the role of environmental constraints is low, the standard expectation is that different taxonomic groups respond in a different way to local habitat and landscape composition. However, in harsher environmental conditions, such as those encountered in mountain areas, climate could act as the main force driving species richness and community composition across all taxa. The role played by temperature in determining species richness, distribution of vulnerable species and partially community composition, as observed in this study,

emphasizes the potential vulnerability of mountain ecosystems to climate warming. In particular, the Alpine belt emerged as a habitat characterised by a peculiar fauna and by a limited number of species which are exclusive to high altitude regions and are highly sensitive to environmental changes.

An added value of this pilot study is the attempt to coordinate a monitoring program among different Natural Parks in the N-W Italian Alps. The results of the program indicated that each protected area, even if it covers a similar altitudinal gradient and has a similar succession of environments, has its own peculiarities in terms of community composition and it is important for conservation purposes. Precise and detailed descriptions of what is present in these protected area, considering different representative taxonomic groups, is thus fundamental to identify conservation goals, both in term of sensitive areas and representative taxa.

Table 2.2.3. Results of Simple and Partial Mantel Tests. For the Simple test, correlations are presented as r-values; * = p < 0.01; ** = p < 0.001; *** = p < 0.0001; n.s. = not significant. The results of the Simple Mantel test are shown in the diagonal with grey background colour. Number of plots = 62, owing to missing temperature values in 7 plots.

	Temperature	Altitude	Belt	Geography	
Carabids	0.228***	(n.s.)	*	***	**Controlling for Temperature**
Butterflies	0.390***	*	***	***	
Spiders	0.316***	(n.s.)	**	***	
Staphylinids	0.245***	(n.s.)	*	***	
Birds	0.398***	***	***	(n.s.)	
Carabids	***	0.178***	(n.s)	***	**Controlling for Altitude**
Butterflies	***	0.350***	***	***	
Spiders	***	0.255***	*	***	
Staphylinids	***	0.204***	(n.s)	***	
Birds	(n.s.)	0.523***	***	**	
Carabids	***	**	0.149***	***	**Controlling for Belt**
Butterflies	***	***	0.354***	***	
Spiders	***	**	0.221***	***	
Staphylinids	***	**	0.149***	***	
Birds	***	***	0.594***	**	
Carabids	***	***	***	0.305***	**Controlling for Geography**
Butterflies	***	***	***	0.285***	
Spiders	***	***	***	0.237***	
Staphylinids	***	***	***	0.164***	
Birds	***	***	***	0.110*	

3. Simulation of temperature increase scenarios

This activity started during the first project year and will be completed in the second year.

The first step in the modelling effort is the development of temperature increase scenarios, in which we will run species distribution models based on presence-only data using Maxent software version 3.3, developed by S. Phillips and colleagues (freely available at http://www.cs.princeton.edu/~schapire/maxent).

The three scenarios which have been developed are:

- 1Degree, in which minimum, mean and maximum temperature are all equally increased by 1° C;
- 1.5Min, in which, minimum temperature is increased by 1.5° C, maximum by 0.5° and mean by 1°;
- 1.5Max, in which minimum temperature is increased by 0.5°, mean by 1°, maximum by 1.5°.

Our choices are supported by the available literature on temperature trends in the alpine areas during the last century, in particular Beniston (2006), which observed a larger increase of minimum temperature, and Ciccarelli et al. (2008), which detected the same increase but for maximum temperature.

We also selected environmental predictors, which will be used to analyse species distribution and to perform model simulations. As environmental predictors, we chose the variables that define micro-climate, altitude, geographic position and vegetation cover conditions, measured in each plot. We combined them in three different ways, to obtain models with an increasing number of environmental constraints:

- *Temp*, in which we consider only temperature-derived parameters and altitude to model species distribution;

- *Tempark*, in which we consider temperature-derived parameters, altitude and geography;

- *All*, in which we consider temperature-derived parameters, altitude, geography and vegetation cover conditions.

Moreover, we identified the species which have enough presence data for our simulation analysis (304 species, 45 Carabidae, 80 Lepidoptera, 99 Araneae, 40 Staphylinidae and 40 Birds).

A conceptual diagram of the modelling effort is shown in figure 2.3.1.

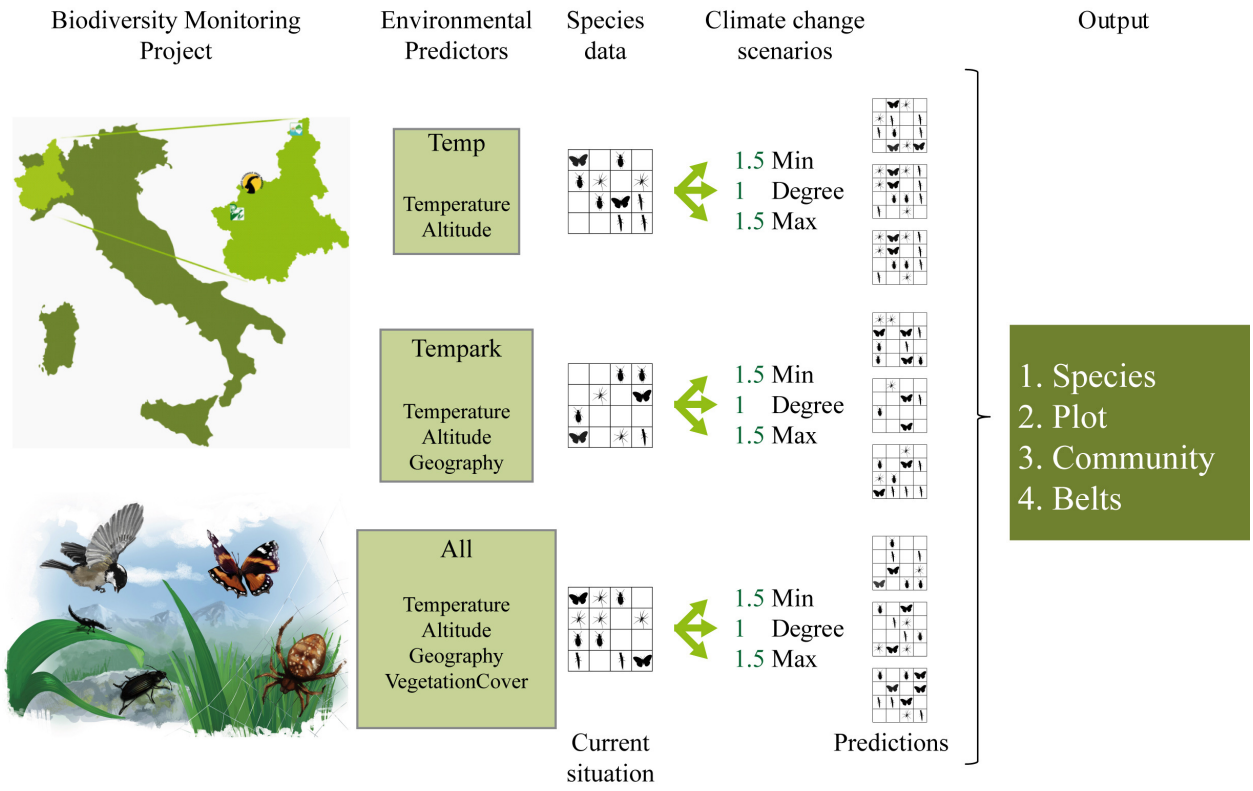

Fig. 2.3.1. Conceptual model idea

All datasets are now ready for running the simulation analysis, which will be performed during the next reference period.

References

Beniston, M. 2003. Climatic change in mountain regions: a review of possible impacts. Climatic Change 59: 5-31.

Beniston, M., 2006. Mountain weather and climate: A general overview and a focus on climatic change in the Alps. Hydrobiologia 562, 3-16.

Bhattarai, K.R., O.R. Vetaas and J. Grytnes. 2004. Fern species richness along a central Himalayan elevational gradient, Nepal. J. Biogeogr. 31: 389-400.

Brehm, J., J. Homeier and K. Fiedler. 2003. Beta diversity of geometrid moths (Lepidoptera: Geometridae) in an Andean montane rainforest. Divers. Distrib. 9: 351-366.

Ciccarelli, N., von Hardenberg, J., Provenzale, A., Ronchi, C., Vargiu, A., Pelosini, R., 2008. Climate variability in north-western Italy during the second half of the 20th century, Global and planetary change 63, 185-195.

Fleishman, E., G.T. Austin and A.D. Weiss. 1998. An empirical test of Rapoport's rule: elevational gradients in montane butterfly communities. Ecology 79: 2482-2493.

Fu, C., X. Hua, J. Li, Z. Chang, Z. Pu and J. Chen. 2006. Elevational patterns of frog species richness and endemic richness in the Hengduan Mountains, China: geometric constraints, area and climate effects. Ecography 29: 919-927.

Grytnes, J.A. 2003. Species-Richness Patterns of Vascular Plants along Seven Altitudinal Transects in Norway. Ecography 26: 291-300.

Hodkinson, I.D. 2005. Terrestrial insects along elevation gradients: species and community responses to altitude. Biol. Rev. 80: 489-513.

Huey, R.B. and R.D. Stevenson. 1979. Integrating thermal physiology and ecology of ectotherms: Discussion of approaches. Am. Zool. 19: 357-366.

Kessler, M. 2002. The elevational gradient of Andean plant endemism: varying influences of taxon-specific traits and topography at different taxonomic levels. J. Biogeogr. 29: 1159-1165.

Kessler, M.S., K. Herzog, T. Fjeldsai and K. Bach. 2001. Species richness and endemism of plant and bird communities along two gradients of elevation, humidity and land use in the Bolivian Andes. Biodivers. Distrib. 7: 61-77.

Körner, C., J. Paulsen and E. Spehn. 2011. A definition of mountains and their bioclimatic belts for global comparisons of biodiversity data. Alp. Bot. 121: 73-78.

Lomolino, J.W. 2001. Elevation gradients of species-density: historical and prospective views. Global Ecol. Biogeogr. 10: 3-13.

Oommen, M.A. and K. Shanker. 2005. Elevational species richness patterns emerge from multiple local mechanisms in Himalayan woody plants. Ecology 86: 3039-3047.

Pauli, H., M. Gottfried, D. Hohenwallner, K. Reiter, R. Casale and G. Grabherr. 2004. The GLORIA field manual. Multi-summit approach. DG Research, EUR 21213, Official Publications of the European Communities, Luxembourg.

Raufaste, N. and F. Rousset .2001. Are partial mantel tests adequate? Evolution 55: 1703-1705.

Rickart, E.A. 2001. Elevational diversity gradients, biogeography, and the structure of montane mammal communities in the intermountain region of North America. Global Ecol. Biogeogr. 10: 77-100.

Sánchez-Cordero, V. 2001. Elevation gradients of diversity for rodents and bats in Oaxaca, Mexico. Global Ecol. Biogeogr. 10: 63-76.

Schmitt, T. 2009. Biogeographical and evolutionary importance of the European high mountain systems. Front. Zool. 6: 1-9.

Vetaas, O. R. and J.A. Grytnes. 2002. Distribution of vascular plant species richness and endemic richness along the Himalayan elevation gradient in Nepal. Global Ecol. Biogeogr. 11: 291-301.

Project of Strategic Interest NEXTDATA

D2.6.c - Results of the pilot study: "Estimation of the changes in the hydrological cycle, snow cover and water availability in high altitude areas"

Prepared by: Silvia Terzago (CNR-ISAC, Torino)

Contributors:
Jost von Hardenberg (CNR-ISAC, Torino), Antonello Provenzale (CNR-ISAC, Torino), Elisa Palazzi (CNR-ISAC, Torino), Adnan Tahir (COMSATS, Abbotabad), Matteo Zampieri (CMCC), Silvio Gualdi (CMCC)

This deliverable is structured as follows: in the introduction we describe the objectives of this pilot study which aims at estimating the recent and future changes in the hydrological cycle, snow cover and water availability in high altitude areas, and we give a general overview on the methodology that will be followed in the course of this pilot study.

In the first part we explore the possibility to use EC-Earth, a state-of-the-art Global Climate Model, for future snow projections. We estimate the EC-Earth accuracy by analysing its capability to describe the present climate, by comparing the snow dataset with the ERA-INTERIM reanalysis.

In the second part we test the possibility to produce snow projections using physical/empirical models in off-line mode, forced by the atmospheric variables produced by the climate models. As in the previous case, we test the models accuracy over a control period. The snow depth simulations in several sites in the Alps and in Siberia are presented and validated through surface observations.

Introduction

This pilot study aims at providing projections of the snowpack characteristics (snow depth, density and areal cover) in the mountain areas, especially the Alps and the Hindu-Kush Karakorum Himalaya (HKKH), for different climate change scenarios, using both global and regional models.

A key step in the study is to determine the methodology that allows to obtain the most reliable snow projections. For this, two different modelling approaches have been identified.

The first approach is to directly use the snow projections provided by the climate models (i.e. EC-Earth), possibly after application of a suitable downscaling procedure. The advantage is

that the atmospheric and the surface-snow modules are interactive and therefore snow change feedbacks on climate can be properly represented.

A second possibility is to use physical/empirical models (i.e. H-Tessel, UTOPIA, degree-day models) in off-line mode. In this approach the snow model is forced by the atmospheric variables produced by the climate model. In this case, the surface-atmosphere feedbacks cannot be represented but, on the other hand, it is possible to calibrate the snow models and, presumably, represent the snow dynamics more accurately for the region of interest.

We are following both approaches, with the aim to determine which is the most effective by comparing the results to the available data. The snow estimates produced by the different methods will be validated with the observations during a control period.

1. Validation of EC-Earth snow products

Concerning the first approach, the snow dataset of the Global Climate Model EC-Earth referring to the historical period 1850-2005 and the projections until 2100 for the scenario RCP4.5 have been collected. The available variables of interest for this study are the snow depth expressed as snow water equivalent and the snow density. From these data, it is possible to reconstruct the snow depth on a global scale, with a spatial resolution of 1.125°, corresponding to about 125 km in the meridional direction and 90 km in the zonal direction at mid-latitudes. We estimated the EC-Earth accuracy in describing the present climate, specifically for the snow variables. Since the EC-Earth dataset is composed of gridded data, the natural basis of comparison is another gridded dataset. The present *state-of-the-art* is the ERA-INTERIM reanalysis (ECMWF), a set of global analysis that assimilates observed data and covers the period since 1979. For a selected case study also the ECMWF analysis product has been considered.

In this study the attention has been focused on the mid-latitudes, in particular the area that extends from Portugal to Japan and that includes the Alps and the Hindu-Kush Karakoram Himalaya (HKKH) mountain ranges (Fig. 3.1.1, Table 3.1.1).

Table 3.1.1. Area of study, reference period, variable and datasets used in the verification of the EC-Earth snow products accuracy.

Area	Lon (-10°E, 130°W) Lat (20°N, 50°N)
Period	1979-2009
Variable	Snow Depth [m of snow water equivalent]
Datasets	ERA-Interim, ECMWF Analysis

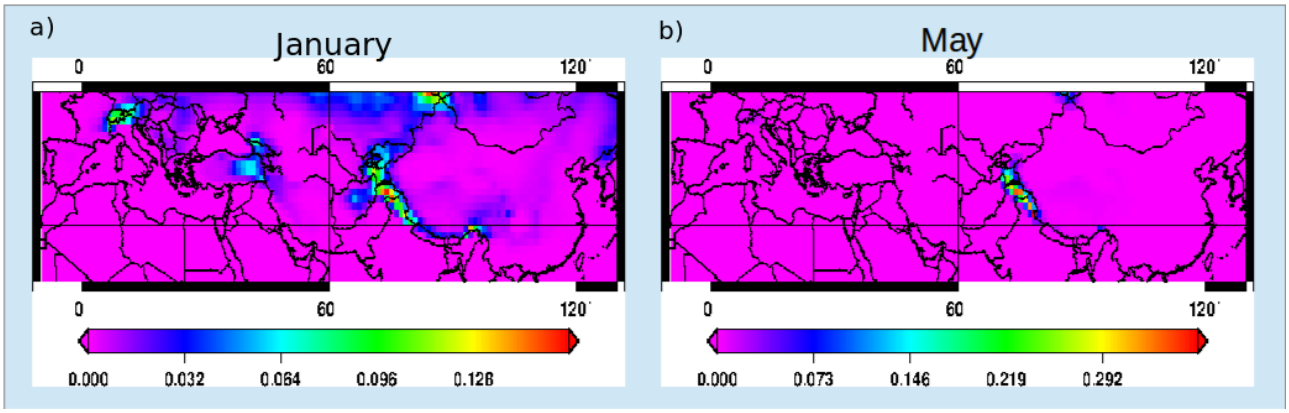

Figure 3.1.1. Climatological average snow depth in January (a) and May (b) from the EC-Earth dataset over the period 1979-2009.

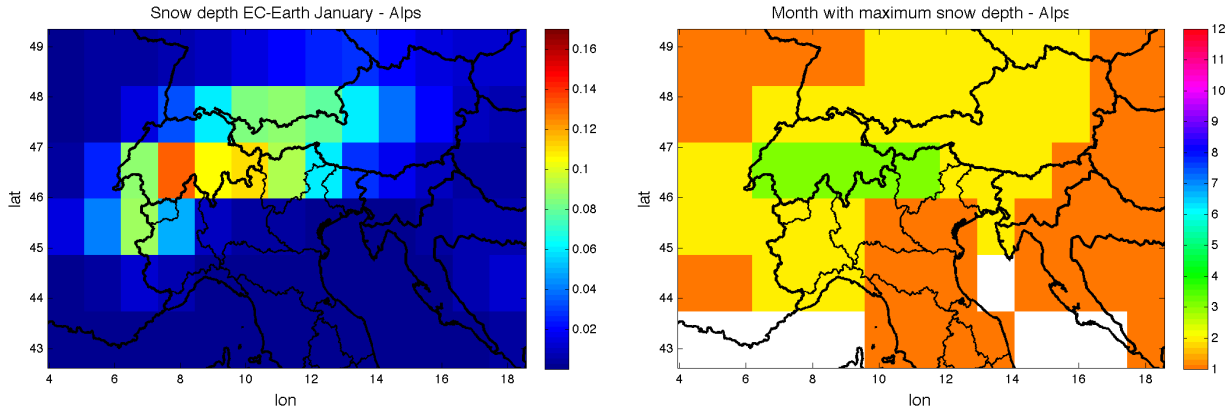

Figure 3.1.2. Average January snow depth in the Alps (period 1979-2009) (left) and month with the maximum snow depth (right) according to EC-Earth dataset. Unclassified pixel (in white) occur when the month with maximum snow depth is not univocally definable.

The analysis of the average snow depth characteristics on a monthly basis allows to determine the variability of solid precipitation, the accumulation and the persistence of snow on the surface throughout the year. It also allows to highlight the differences between climatic sub-regions in the area of interest. The comparison of the average snow depth in January and May (Fig. 3.1.1) shows that in the Alps the maximum snow accumulation occurs in winter, afterwards the snow depth decreases and in May the surface is almost totally snow-free. On the contrary, in the HKKH region, due to the higher average altitude, the accumulation continues even after the winter months and reaches a maximum in spring.

Figure 3.1.2 (left) shows in detail the average snow depth in the Alps and Fig. 3.1.2 (right) represents the month when the maximum snow depth occurs. At increasing altitude, the maximum occurs later and shifts from the winter (January/February) to the spring (March) months.

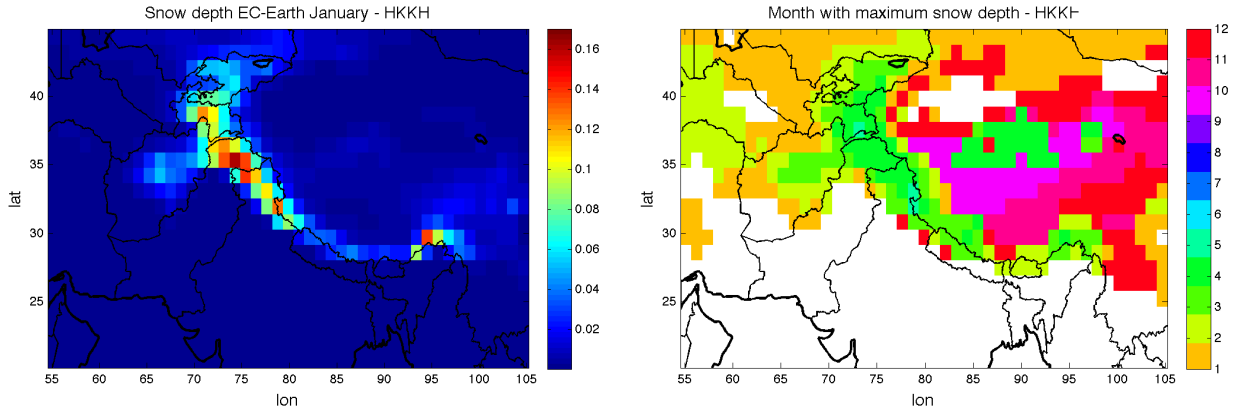

Figure 3.1.3. Average January snow depth in HKKH (period 1979-2009) (left) and month with maximum snow depth (right) according to EC-Earth dataset. Unclassified pixel (in white) occur when the month with maximum snow depth is not univocally definable.

In the HKKH area, the month with maximum snow depth varies depending on geographical factors (Fig. 3.1.3, right). In the North-Western area and in the Hindu Kush mountains (Afghanistan), the highest snow depth occurs in the winter, in January and February. In the area of the Karakoram/Baltoro mountains, the maxima are recorded in spring, in March/April, while over the highest peaks the maxima occur in May. Downstream of these mountain ranges the maxima are registered in winter, from October to December.

EC-Earth maps of monthly average snow depth in the period 1979-2009 have been compared with the corresponding ERA-Interim reanalysis dataset. An inconsistency has been found in the Karakoram region, at the border between Pakistan and China, in the area of the Baltoro glacier. With mean length of 62 km and an area of 640 square kilometers approximately the Baltoro glacier is one of the largest glaciers in the world. Within 20 km there are K2, the highest mountain in the region, and three other peaks above 8,000 m s.l.m. In this area ERA-Interim estimates about 7 meters of snow water equivalent, while EC-Earth values are about an order of magnitude lower. This significant difference is recorded throughout the year, regardless of the month. Fig. 3.1.4 shows the maps for January.

The large discrepancy between EC-Earth and ERA-Interim can be explained by different choices in the snow schemes and in particular by a different treatment of glaciers. In ERA-Interim, a static glaciers mask is adopted to force the snow depth at a constant value of 10 meters over glaciers, while this choice is not adopted in EC-Earth. The 10-m value is not representative of the real conditions in the Baltoro area, thus the EC-Earth snow fields should be compared with other independent snow datasets. To our knowledge, however, no historical long-term climate series is available for the Baltoro glacier region owing to its impervious and scarcely accessible territory.

Recently some sparse nivo-meteorological observations have been performed during specific measurement campaigns organized through high altitude expeditions. Among them there is the campaign of the international project PAPRIKA that sampled 3 snow-pits to study the snowpack characteristics along the vertical, from the snow surface to the soil. The maximum snow depth observed in these 3 observations was about 8 m and the average density was 400 kg/m^3, corresponding to a 3.2 m snow water equivalent. We point out that this measure is of the same order of magnitude of ERA-Interim estimate, however, it is very difficult to infer the spatial representativeness of this data and further measurements in that area are necessary.

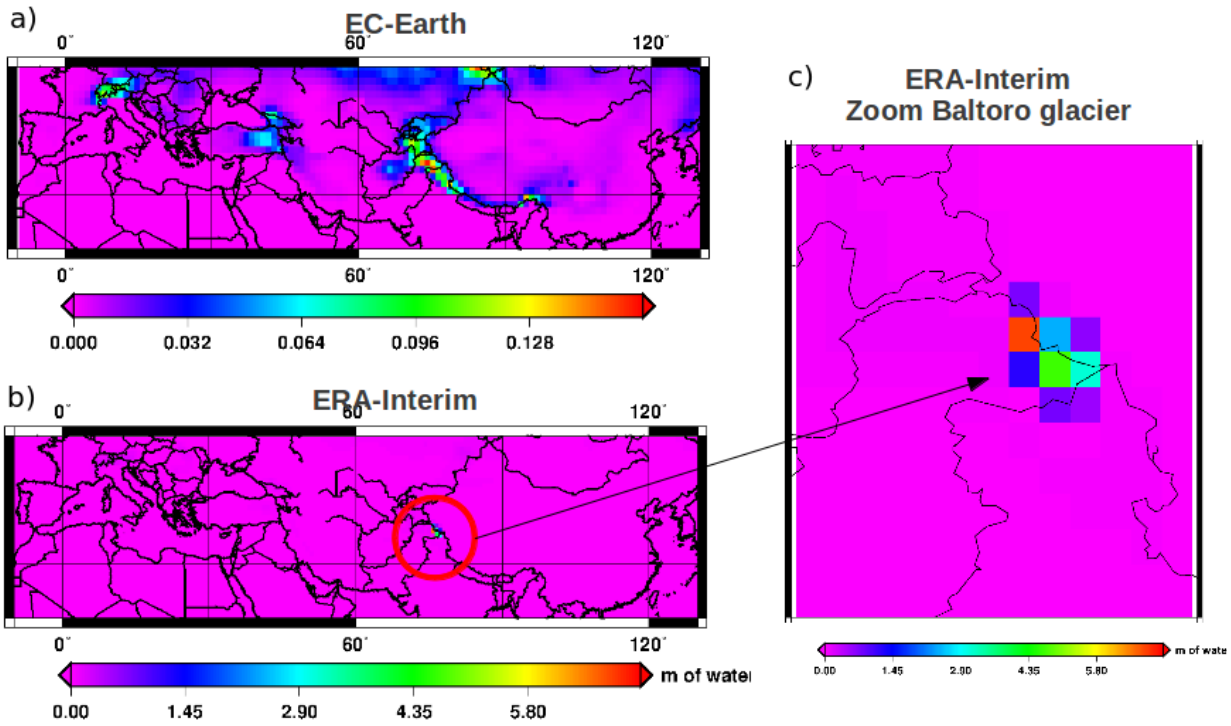

Figure 3.1.4. Monthly average snow depth, expressed in meters of water equivalent, according to EC-Earth (a) and ERA-Interim (b) over the period 1979-2009. ERA-Interim presents a maximum in the Baltoro area (c) of about one order of magnitude higher than EC-Earth.

Another measurement site activated in the Baltoro area is the Concordia automatic weather station, installed by the Ev-K2-CNR Committee in collaboration with the Pakistan Meteorological Department (PMD). The station, located at 4700 m above sea level, measures since 2012 the total precipitation, snow depth, wind speed and direction, air temperature, relative humidity, solar and terrestrial (long and short-wave) radiation and net radiation. Figure 3.1.5 shows the daily air temperature and snow depth measurements between 18 January 2012 and 5 November 2012. The maximum snow depth recorded is about 2 meters, so it is much lower than the one derived by the snow-pit.

Two more stations have been installed by Ev-K2-CNR, in collaboration with PMD, in the Baltoro area, at Urdukas (3926 m a.s.l.) and Askole (3015 m a.s.l.) in 2004 and 2005 respectively. These stations provide continuous data of the main meteorological variables, but precipitation measurements are discontinuous and they are not performed during most of the winter months. The solid precipitation is not measured and therefore, to date, there are no other nivometrical measures at these two sites.

Through the literature search and the establishment of contacts with research institutions in Pakistan, we obtained the daily data of 10 hydro-meteorological stations managed by the Water and Power Development Authority (WAPDA) and located in the Karakoram area (Fig. 3.1.6). The measured variables are the maximum and minimum temperatures, the maximum and minimum relative humidity, the accumulated precipitation, the snow water equivalent (SWE) and the total solar radiation. This is a valuable dataset, both for the amount of data and for the location of the stations, all between 2000 and 5000 m above sea level.

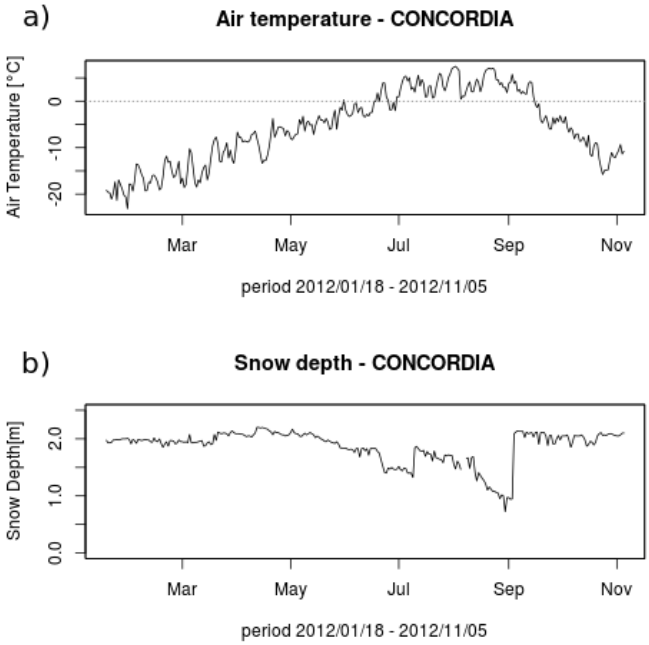

Figure 3.1.5. Daily air temperature (a) and snow thickness (b) measurements at the Concordia station (Pakistan, 4700 m a.s.l.) between 18 January 2012 and 5 November 2012.

As part of this study we explored the cumulated snow water equivalent series and we detected several inconsistencies in the data temporal variability. There are negative - and therefore incorrect - data, suspect peaks, abrupt changes in SWE and, more generally, several inhomogeneities in the data collection. The series require a careful quality check to identify the erroneous data before starting a statistical analysis.

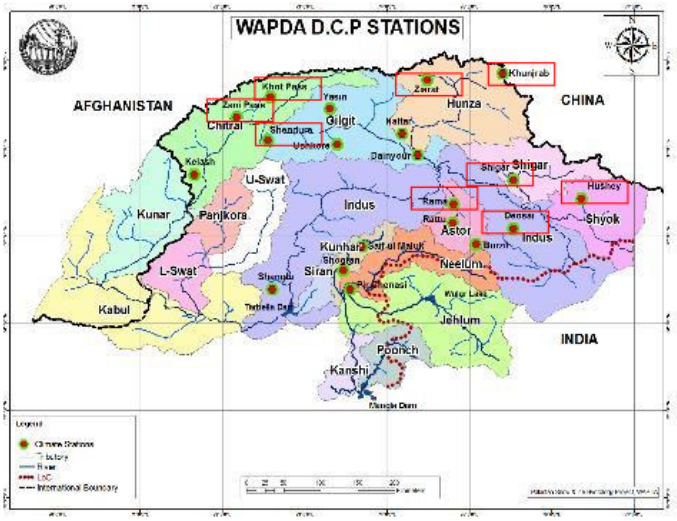

Figure 3.1.6. Map of the hydro-meteorological stations managed by the Water and Power Development Authority (WAPDA) in northern Pakistan, Karakoram mountains. The considered stations are highlighted by red boxes.

Excluding the Baltoro area to which we will devote further research, we compared the monthly maps of EC-Earth with ERA-INTERIM, pixel by pixel. In order to evaluate the relationship between each pair of maps, we plotted the EC-Earth values in function of the ERA-INTERIM ones. Figure 3.1.7 shows the scatterplot for the months of January, April and August.

The correlation between the two climatologies depends on the season. In January, the correlation coefficient is R2=0.60 and, compared to ERA-INTERIM, EC-Earth tends to underestimate the snow depth, probably as a consequence of the underestimation of the total precipitation (Palazzi et al., 2013). In April, the correlation between the two datasets decreases (R2=0.40). In spring, EC-Earth overestimates the snow thickness due to a delayed snow melting. In August, the two datasets are uncorrelated, in particular EC-Earth does not properly distinguish between snow-covered and snow-free areas and it produces a very shallow snow depth in summer.

In conclusion, the analysis of the historical period 1979-2009 shows that EC-Earth and ERA-INTERIM snow climatologies are comparable in winter but they exhibit important discrepancies in spring/summer.

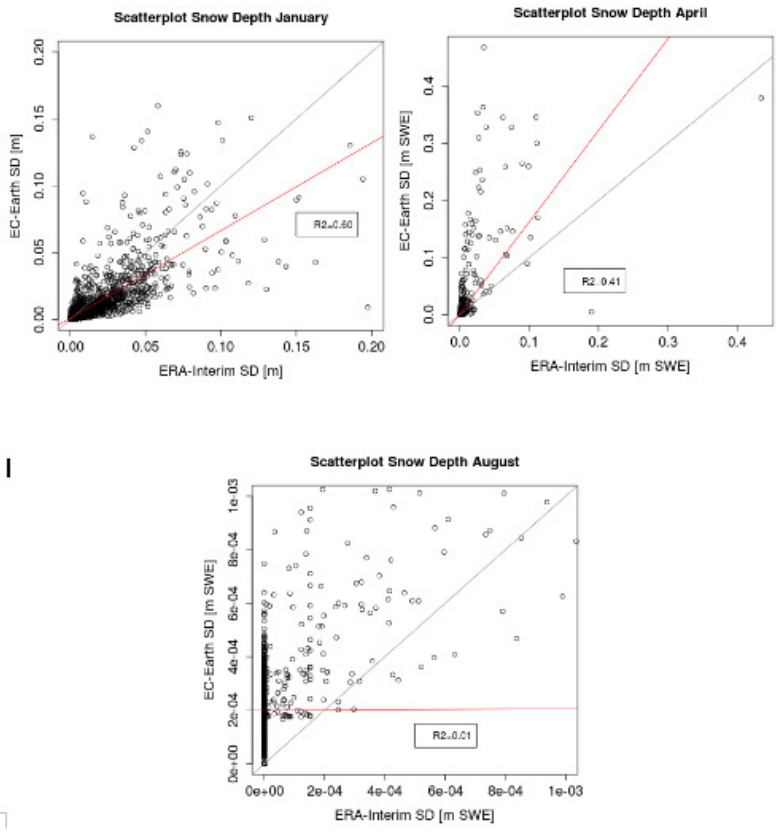

Figure 3.1.7. Scatterplot of the average monthly snow depth in EC-Earth vs. ERA-INTERIM in January, April and August (clockwise order) in the area of study. The Baltoro area has been excluded from the analysis.

2. Evaluation of snow models

Literature research allowed us to identify the physical and empirical models that simulate the temporal evolution of the snowpack, i.e. the accumulation, transformation and fusion processes, using meteorological variables. These distributed models can be applied to simulate the evolution of spatial distribution of snow depth.

The physical models reproduce the exchange processes between the surface and the atmosphere and are based on the energy and hydrological balance equations at the Earth's surface. These models can have different degrees of complexity, but they generally require several input variables, such as temperature, pressure, humidity, precipitation, wind direction and wind speed, solar radiation and they are quite demanding from the point of view of the computing resources. On the other hand, they can reproduce many of the snow processes and

snow-related variables (snow depth, density, water equivalent, snow temperature at various depths, etc ...).

Empirical models estimate the solid precipitation fraction and the amount of melted snow through empirical relations between temperature and precipitation, which are usually the only two input meteorological variables needed. These models, although very simple, may be able to reproduce with good accuracy the snow behavior and they have the advantage of requiring only two easily available input variables, and few computational resources.

After a literature search we identified different physical (UTOPIA, CHTESSEL, FEST, GEOTOP, ACHAB-Snow) and empirical (SNOW17 ETI) models and we studied the related articles. We focused on the UTOPIA model as it was immediately made available by the developers of the University of Torino. Recently we acquired also CHTESSEL, the currently operational model at ECMWF and also integrated in EC-Earth. These two models have been installed on a computer at CNR-ISAC in Torino and they are now available for simulations. We also established contacts with the CIMA Research Foundation in Savona to obtain the ACHAB-Snow surface model, that will be made available shortly.

The research that we are pursuing aims at comparing the different models and at assessing their accuracy in different geographical contexts, both Alpine and extra-Alpine. Initially, we carried out simulations based on surface stations data. In the Piedmont Alps there are 10 meteorological stations that measure all the necessary variables including snow (Fig. 3.2.1) and their data have been requested to the managing agency ARPA Piemonte.

Stazioni	Quota [m slm]	Disp. dati
Passo del Moro	2820	1988
Sestriere Banch.	2480	2003
Sestriere Alpette	2250	2003
Colle Bercia	2200	1996
Clot della Soma	2150	1996
Limone Pancani	1875	2006
Rifugio Mondovì	1760	1997
Pragelato	1620	2002-2010/07
Prerichard	1353	1990
Settepani	1300	2003
Ponzone Bric B.	773	1989

Figure 3.2.1. List of the snow-meteorological stations of the ARPA Piemonte network that are fully instrumented. Elevation and period of data availability are also reported. The station of Limone Pancani was activated in 2006 and has the shortest record, the others are operating at least since 2003.

Figure 3.2.2 (left) shows a snow depth simulation at Colle Bercia station (2200 m a.s.l.) obtained using the UTOPIA model. It can be seen that the model adequately reproduces the snowfall and melting processes, with a tendency to underestimate snowfall in the case of intense events. But we have to remind that the amount of solid precipitation is determined in UTOPIA from heated rain gauges measurements. These instruments are designed for measuring the liquid precipitation and they tend to underestimate solid precipitation. In fact their resistor is not able to melt quickly enough the snow that tends to accumulate and to obstruct the lens, producing a remarkable underestimation during intense events. In addition, the instrument itself tends to deflect the wind and reduce the amount of snow captured by the gauge. Thus, the deviation between the UTOPIA simulation and the real snow depth may be partly due to the quality of the initial precipitation data rather than uniquely to an internal

problem of the model. The complete snow melting simulated by UTOPIA occurs about 7 days later than the observations, thus the model tends to retain snow longer.

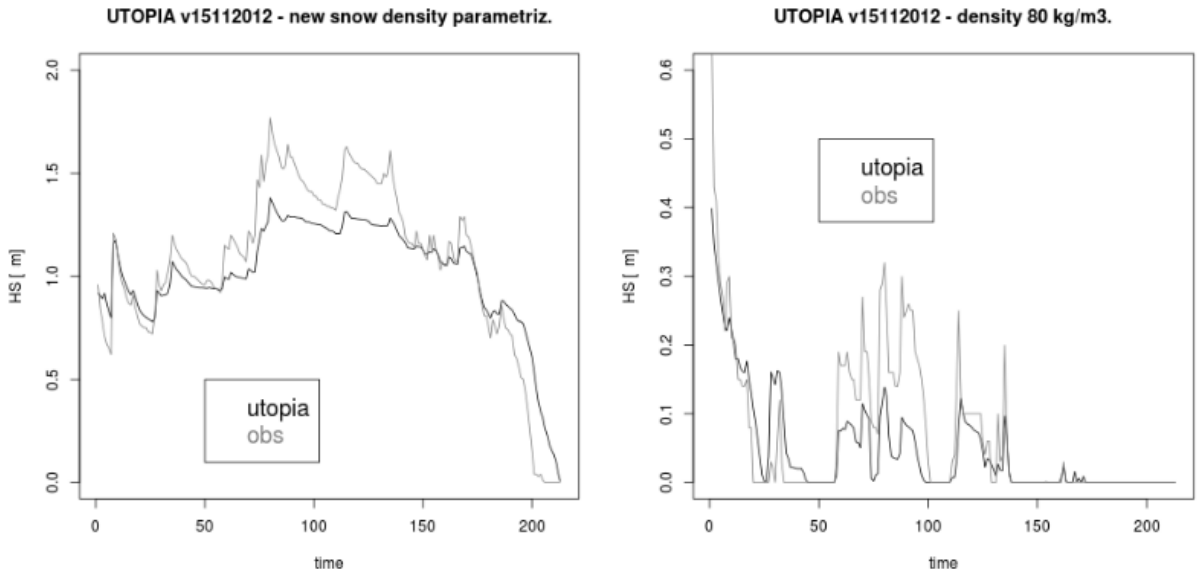

Figure 3.2.2. UTOPIA-simulated snow depth (black line) and observation (gray line) in Colle Bercia (left) and Prerichard (right) stations in the Piedmont Alps, starting from November, 1 2003 until May, 31 2004.

The same analysis was performed on the Prerichard station, located at 1353 m above sea level (Fig. 3.2.2, right). UTOPIA faithfully reproduces the processes in the early snow season and, similarly to the case of Colle Bercia, it underestimates the solid precipitation during snowfalls exceeding 20 cm.

To verify the functioning of the model, we also carried out some tests also on two Siberian meteorological stations (Fig. 3.2.3):

- Ogurtsovo 54 ° 54 'N lat., 82 ° 57' E long, altitude 133 m above sea level
- Kostroma 57 ° 46 'N lat., 40 ° 56' E long.; 126 m

the complete datasets are freely available online (http://rp5.ru/Weather archive in Ogurtsovo http://rp5.ru/Weather archive in Kostroma).

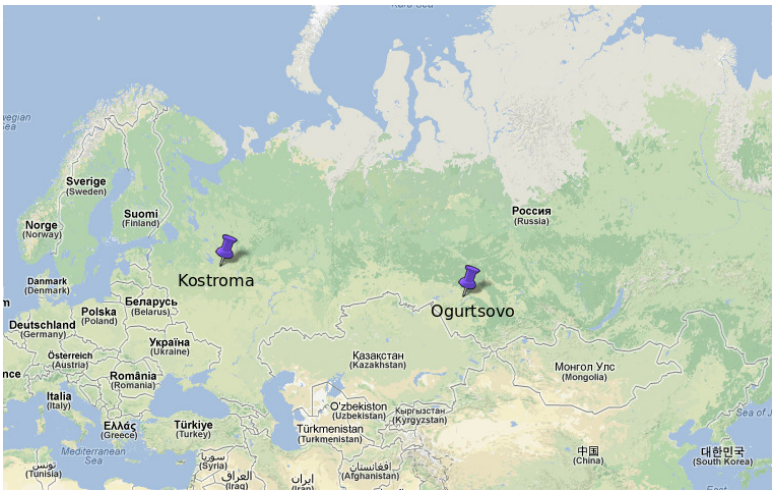

Figure 3.2.3. Location of the two Siberian stations of Kostroma and Ogurtsovo considered in the study.

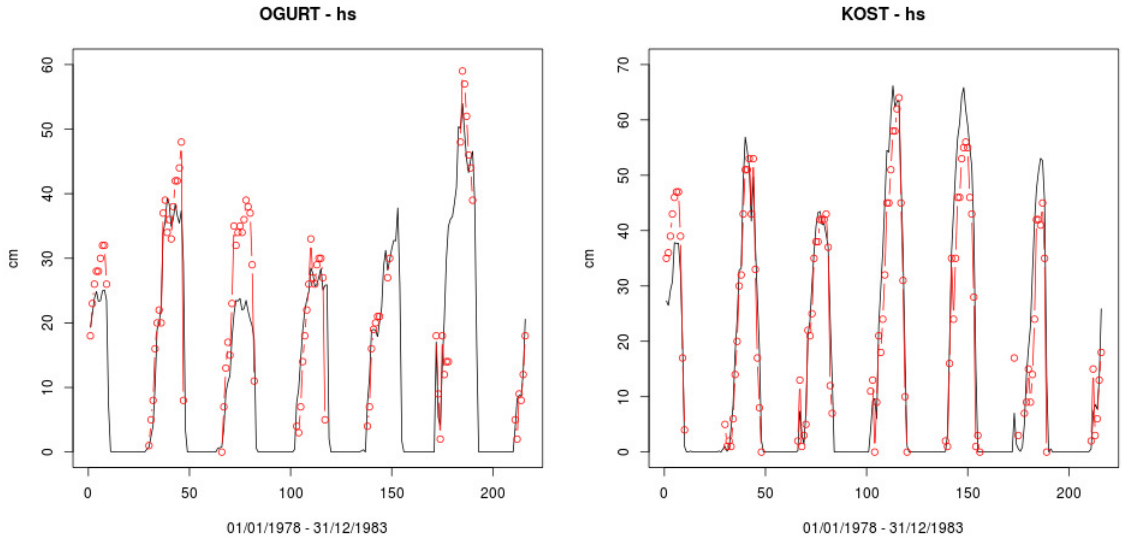

Figure 3.2.4. Time evolution of the snowpack simulated by UTOPIA (black line) and observed (red line with circles) in Ogurtsovo (left) and Kostroma (right) stations (Siberia), from January, 1 1978 until December, 31 1983.

Simulations have been performed using 30' time series from 1st January 1978 to 31st December 1983. The results are shown in Fig. 3.2.4: in Ogurtsovo the UTOPIA simulations reproduce quite well the observed signal throughout the period considered with the exception of the 1979-80 season, when the snowfall is underestimated by approximately 30 cm.

The best results are obtained in the station of Kostroma where there is a good agreement between the real and the reconstructed signal. In this case UTOPIA reproduces the observed data with high accuracy.

After the encouraging results obtained with Utopia on sample stations, in the near future other snow models will be tested and evaluated through a comparative analysis to determine their relative accuracy.

3. Snow precipitation variability in the Alpine area

In the framework of this pilot study, CMCC has initiated and developed a series of analyses investigating the variability of seasonality of precipitation and the liquid to solid precipitation ratio and their effects on the hydrological cycle of the region. To this purpose, an analysis of the observed long-term discharge time-series of the Rhine, the Danube, the Rhone and the Po rivers has been performed.
Figure 3.3.1 shows the geographical distribution of the four stations and the relative river basins upstream, covering most of the Alps. River discharge monthly time-series are obtained by blending different sources, mainly from the Global Runoff Data Center (GRDC, http://www.bafg.de) and from local regional authorities. For the analysis of the snow variability, gridded datasets of monthly homogeneized surface observations developed in the HISTALP project and available at 10' resolution from 1801 to 2003 for precipitation and from 1870 to 2008 for temperature (Efthymiadis et al 2006, Auer et al., 2007, see Brunetti et al 2009 for an analysis of trends and variability) are going to be used.

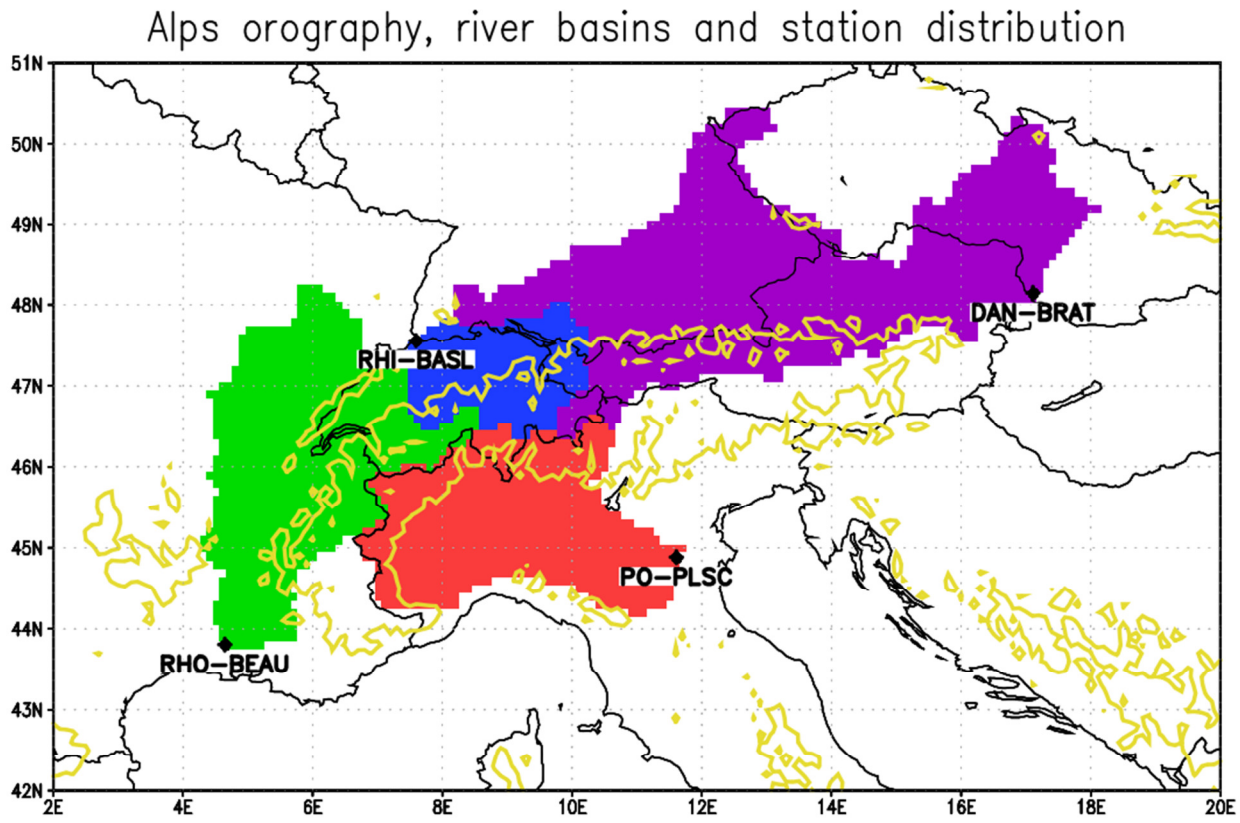

Figure 3.3.1. Distribution of the four stations that we selected as representative of the four major Alpine rivers and basins: the Rhine river in Basel (RHI-BASL, 7.59E-47.55N, blu basin), the Danube river in Bratislava (DAN-BRAT, 17.11E-48.14N, violet basin), the Rhone river in Beaucaire (RHO-BEAU, 4.64E-43.81N, green basin) and the Po river in Pontelagoscuro (PO-PLSC, 11.60E-44.89N, red basin). The basin delineations plotted in the figure, which we generated using a 5' (about 7.5 km) river direction dataset (Graham et al 1999), are remapped at 10' resolution consistently with the resolution of the climatic data that we adopt in this study. The yellow contour line depicts the 1000 m altitude of the orography.

These rivers are characterized by different seasonal cycles reflecting the different climates and morphologies of the Alpine basins. Many studies focused on the mean climatology, seasonal trends and extremes of the discharge intensities of these rivers, often in connection with sediment transport, ecology, or human-related activities (see e.g. Eckhardt and Ulbrich 2003, Pekárová et al. 2003, Birsan et al. 2005, Zanchettin et al 2008, Beniston et al. 2011, Hänggi and Weingartner 2011, Szczypta et al. 2012).

In our study, on the other hand, we focus on the spring discharge timing, which is an important indicator of the hydrological cycle affecting many natural and anthropic systems. We define it as the time of the year with the first maximum river discharge (based on a fitting procedure with the monthly data). Figure 3.3.2 shows the low frequency variability of the spring discharge timing in the four stations, together with the standard deviation associated to the high frequency variability after the time-smoothing of the time-series.

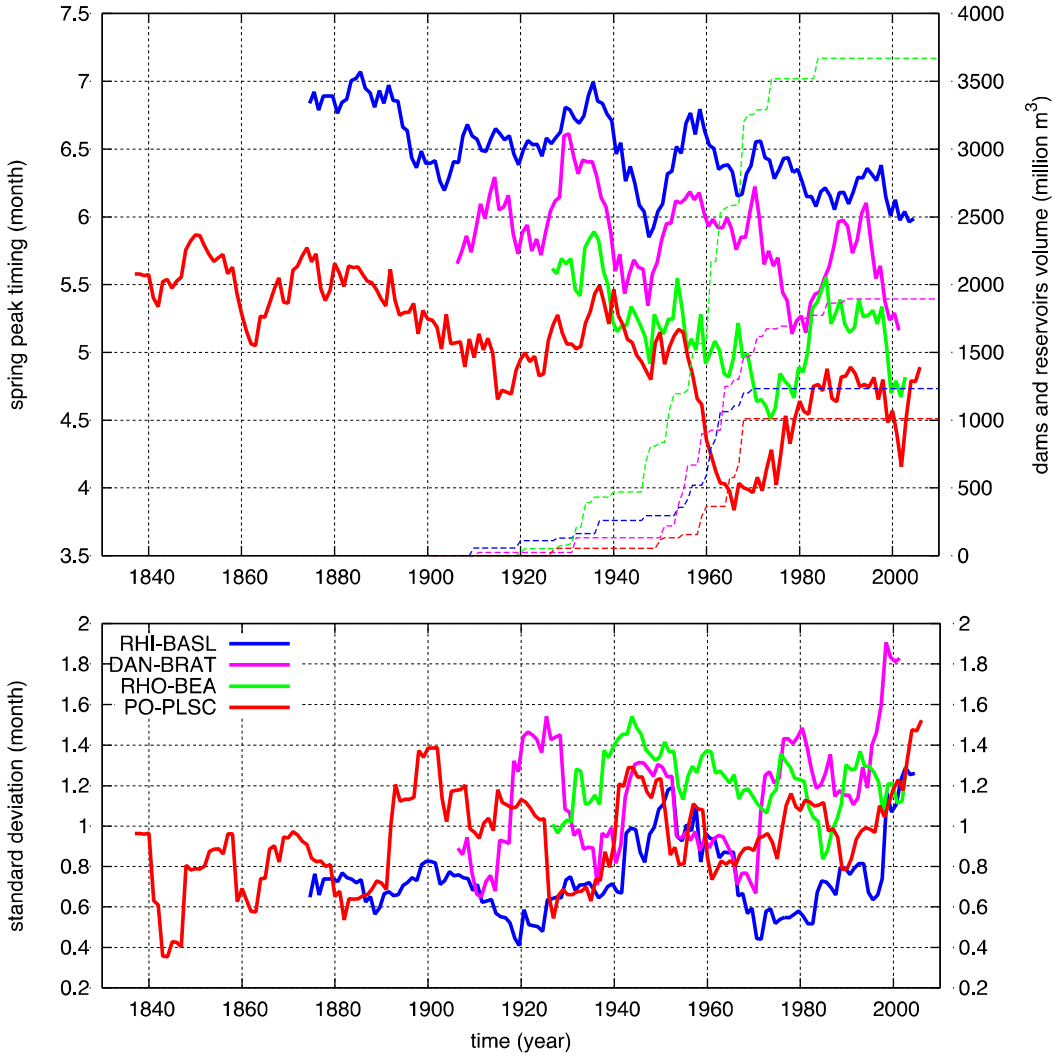

FIG. 3.3.2: 11 years running mean phases time series of the fitting functions (top panel) and the associated standard deviation computed on the same time window (bottom panel). Dashed lines on top panel represent the accumulated dam and managed reservoirs volume in the basins upstream the stations, computed using the Global Reservoir and Dam (GRanD) database (Lehner et al 2011).

Despite the intensive water management in this region, we found common features in the spring discharge timing trend and low-frequency variability in the different basins. All time-series display an anticipating tendency of the spring discharge peaks of more than two weeks per century. These results can be explained in terms of changes in snowmelt timing, in total precipitation and of its liquid portion, which play different roles in the different basins. A paper illustrating and discussing the results found in this analysis is in preparation.

Due to the lack of comprehensive hydrological measurements at this spatial and temporal scales, a series of experiments with climate models are going to be analyzed in order to explore the mechanisms underpinning the observed variability. Since the river discharge is not a standard model output, future analysis will be focused on the runoff generated in the basins, total precipitation and rainfall to snowfall ratio.

Conclusions

This study aims at providing projections of the snowpack characteristics (snow depth, density and areal cover) in the mountain areas of interest to the project, especially the Alps and the HKKH region. Two different research approaches have been identified: (i) use of the snow

projections provided by the EC-Earth Global Climate Model and (ii) running physical/empirical models in off-line mode, forced by the atmospheric variables produced by the climate model.

Concerning the first approach, the correlation between the EC-Earth snow dataset and the ERA-INTERIM reanalysis over the historical period 1979-2009 strongly depends on the season. It is higher in winter (R^2=0.6) than in summer when EC-Earth is not able to correctly reproduce the spatial distribution of snow depth. This analysis suggests that EC-Earth might underestimate the snow depth over the Baltoro area, in the Karakoram mountains. The lack of surface observations makes difficult to draw conclusion on the real snow depth in this key-area, so new measurements should be performed in the future.

Concerning the second approach, we collected several physical snow models and performed some simulations with UTOPIA to determine its accuracy in several sites in the Alps and in Siberia using surface observations. The model adequately reproduces the snowfall and melting processes, with a tendency to underestimate snowfall in the case of intense events. It is worth to mention that this discrepancy may be partly due to an underestimation of the initial precipitation rather than uniquely to an internal problem of the model. The best results are obtained in Siberia where there is a good agreement between the real and the reconstructed signal. In the near future we will implement a larger dataset including other Alpine and HKKH sites where meteorological parameters are available. The dataset will be the benchmark to test and compare the performances of different physical/empirical snow models.

Since we want to carry out simulations driven by the output of global/regional climate models, we will have to work on gridded data at low spatial resolution. So we will study the sensitivity of the snow models to the degradation of the spatial resolution of the initial data. We plan to carry out simulations with different types of input data, of gradually decreasing "quality", starting from (i) the ideal case when all input variables are available (data from the fully equipped weather stations), then (ii) the case when only the main variables are provided (data from the standard meteorological stations) and the others are estimated directly by the model through its own parameterizations, and finally (iii) using interpolated datasets with low spatial resolution and larger uncertainty. This survey will identify the models that provide the best estimates when the input data are forced by low spatial resolution. These models will be used to produce snow projections for the following decades.

References

Auer I, Böhm R, Jurkovic A, Lipa W, Orlik A, Potzmann R, Schöner W, Ungersböck M, Matulla C, Briffa K, Jones PD, Efthymiadis D, Brunetti M, Nanni T, Maugeri M, Mercalli L, Mestre O, Moisselin J-M, Begert M, Müller-Westermeier G, Kveton V, Bochnicek O, Stastny P, Lapin M, Szalai S, Szentimrey T, Cegnar T, Dolinar M, Gajic-Capka M, Zaninovic K, Majstorovic Z and E Nieplova 2007 HISTALP – Historical instrumental climatological surface time series of the greater Alpine region 1760-2003 Int. J. Climatol. 27 17-46.

Beniston M, Stoffel M and M Hill 2011 Impacts of climatic change on water and natural hazards in the Alps: can current water governance cope with future challenges? Examples from the European "ACQWA" project Environ. Sci. Policy 14 734-43

Birsan M V, Molnar P, Burlando P and M Pfaundler 2005 Streamflow trends in Switzerland. J. Hydrol. 314 312-29

Brunetti M, Lentini G, Maugeri M, Nanni T, Auer I, Böhm R and W Schöner W 2009 Climate variability and change in the greater alpine region over the last two centuries based on multi-variable analysis Int. J. Climatol. 27 17-46

Efthymiadis D, Jones P D, Briffa K R, Auer I, Böhm R, Schöner W, Frei C and J. Schmidli 2006 Construction of a 10-min-gridded precipitation data set for the Greater Alpine Region for 1800-2003 J. Geophysi. Res. 110 D01105

Eckhardt K and U Ulbrich 2003 Potential impacts of climate change on groundwater recharge and streamflow in a central European low mountain range J. Hydrol. 284 244-252

Graham S T, Famiglietti J S and D R Maidment 1999 Five-minute, 1/2º, and 1º data sets of continental watersheds and river networks for use in regional and global hydrologic and climate system modeling studies Water Resour. Res. 35 583-7

Lehner B, Liermann C. Revenga C, Vörösmarty C, Fekete B, Crouzet P. Doll P. Endejan M, Frenken K, Magome J, Nilsson C, Robertson J C, Rodel R, Sindorf N and D Wisser 2011 Global Reservoir and Dam Database, Version 1 (GRanDv1): Reservoirs, Revision 01. NASA Socioeconomic Data and Applications Center (SEDAC): http://sedac.ciesin.columbia.edu/data/collection/grand-v1

Pekárová P, Miklánek P and J Pekár 2003 Spatial and temporal runoff oscillation analysis of the main rivers of the world during the 19th-20th centuries J. Hydrol. 274 62-79

Szczypta, C., Decharme, B., Carrer, D., Calvet, J.-C., Lafont, S., Somot, S., Faroux, S., and Martin, E.: Impact of precipitation and land biophysical variables on the simulated discharge of European and Mediterranean rivers, Hydrol. Earth Syst. Sci., 16, 3351-3370

Zanchettin D. Traverso P and M Tomasino 2008 Po River discharge: a preliminary analysis of a 200-year time series Climatic Change 89 411-33

Project of Strategic Interest NEXTDATA

D2.6.d - Results of the pilot study:
"Effect of aerosols in high altitude areas"

Prepared by: Jost von Hardenberg (CNR-ISAC, Torino).

Contributors: Elisa Palazzi (CNR-ISAC, Torino), Antonello Provenzale (CNR-ISAC, Torino), Fabien Solmon (ICTP, Trieste), Filippo Giorgi (ICTP, Trieste)

This deliverable is structured as follows: we first summarize and discuss the main physical mechanisms involving aerosols in climate and their role in high-altitude areas, in particular the Hindu-Kush - Karakoram - Himalaya region (HKKH). We then focus on a description of numerical modelling results for the study area, using a regional climate model (the RegCM3 model) and a comparison in terms of aerosol optical depth (AOD) with available satellite and reanalysis datasets.

In this deliverable, ICTP has performed and provided the regional climate model (RCM) simulations and has participated in the analysis of the results. CNR-ISAC has provided the EC-Earth global climate model runs used as boundary conditions for the RCM, participated in the analysis and compiled an overview of the existing in-situ datasets and literature.

1. Introduction and state of the art

The Hindu-Kush Karakoram Himalaya (HKKH) is the largest mountain region in the world, it contains a large amount of glacier ice and plays a crucial role in the hydrologic balance of South-East Asia, providing significant amounts of melt water, especially in the dry season, for agriculture, drinking purposes and power production (Akhtar et al. 2008, Hewitt 2005, Immerzeel et al. 2010).

Both natural and anthropogenic aerosols have a significant impact on the climate and on the hydrological balance in this region. Most Himalayan glaciers have been found to retreat or loose mass in recent years, due to both a significant regional warming trend and to the impact of a severe load of atmospheric aerosols. This region confines with the most densely populated areas of India and China, and it is exposed to the transport of heavy pollution originating from increasing industrial activities and traffic in these areas in recent years (UNEP 2008). In addition to its exposure to anthropogenic aerosols, the HKKH mountain ridge is surrounded by desert areas (eg. Thar, Kara-Kum, Kyrgyl-Kum, Takla Makan regions) and the influence of pollution aerosols on size distribution, concentration and chemical composition of particulate matter is very likely augmented by the presence of mineral dust. In fact, the entire South Asian region is characterized by the presence of the so-called Atmospheric Brown Cloud (ABC**;** Ramanathan et al. 2001), a brownish haze that covers and envelopes this region, which can be attributed both to natural and anthropogenic aerosol emissions, including severe biomass burning and fossil fuels.

A crucial climatic effect of aerosol is from the so-called "direct effect", in which aerosols scatter and/or absorb the solar radiation, thus cooling the Earth's surface and changing the radiative balance of the atmosphere. Aerosols also affect the water cycle through so-called "indirect effects", increasing the number of cloud condensation nuclei, inhibiting the growth of cloud drops to raindrops and increasing the lifetime of clouds. This leads to more persistent and less precipitating clouds, increase reflection of solar radiation and further cool the Earth's surface. While most aerosol components scatter solar radiation, black carbon (BC) and, to a lesser extent, mineral dust, absorb solar radiation. Large amounts of these aerosols characterize the Atmospheric Brown Cloud (ABC) and have been revealed at high altitude in the eastern Himalaya (Nepal Climate Observatory - Pyramid ABC site, Nepal) (Bonasoni et al., 2008; ACPD Special Issue, 2009). Studies on the Atmospheric Brown Cloud have shown that this haze blocks up to 15 % of solar radiation, causing cooling of the surface and heating of the atmosphere, which can affect monsoons and other rainfall patterns (Ramanathan et al. 2005). This kind of brown haze has assumed continental scale proportion; moreover in tropical area, the presence of a dry season can increase aerosol and cloud lifetime and thus enhance both direct and indirect effects (Lau et al. 2006).

When deposited on a glacier surface, the dark aerosols lower glacier albedo and favour ice melt. Light-absorbing aerosols such as black carbon and dust decrease the surface albedo of snow and ice (Warren and Wiscombe, 1980; Clarke and Noone, 1985), an effect causing substantial positive radiative forcing (Hansen and Nazarenko, 2004; Flanner et al., 2007). The dimming of surface insolation due the presence of these aerosols in the atmospheric column is largely compensated by increased surface absorption due to the darkening of snow and ice from deposited soot (Flanner et al. 2009), leading to a positive surface forcing. As a consequence, in the Arctic and in the Himalayas, deposited carbon is found to contribute significantly to seasonal snow melting, snow aging and glacier reduction (Flanner et al. 2009, Menon et al. 2010, Kopacz et al. 2010). These processes lead to a global snow/ice/climate feedback but also, particularly in the Himalayas, to critical changes in the local hydrology and water availability. On a global scale the indirect effects associated with deposition of carbonaceous particles on snow and ice, leading to changes in the surface albedo, snow temperature and structure, have been recognized to represent a significant fraction of the global climatic forcing of these aerosols (Holland and Bitz, 2003, Hansen and Nazarenko, 2004, Flanner et al. 2007, Ramanathan and Carmichael, 2008).

Two important climate feedback mechanisms associated with aerosols over the Indian subcontinent have been widely discussed in recent literature. Ramanathan et al. (2005) discussed a possible reduction of rainfall due to increased thermal contrast between the Indian ocean and the continent, due to surface dimming effects, while Lau et al. (2006) and Lau and Kim (2006) discussed a possible strengthening of the Indian monsoon due to upper tropospheric warming in late spring, due to absorbing dust and black carbon. These mechanisms have been questioned in recent studies (Nigam and Bollasina, 2010; Gautam et al., 2009) which, based on observation data, highlighted the importance of semi-direct effects such as heating of the land surface and of regional and seasonal aerosol distributions.

This debate highlights the importance of modelling and of simulating with high spatial resolution and adequate parameterizations the long-range transport mechanisms and the dynamics of aerosols in this region. While global climate models may provide a first crucial information, it is particularly with regional climate models which include the dynamics of aerosols that this problem can be addressed. In the following we describe an implementation and a preliminary analysis focusing on Aerosol Optical Depth of RegCM4 regional climate model experiments, for the HKKH region.

2. Modeling Aerosol optical depth with a regional climate model

The RegCM4 Regional Climate model

RegCM4 represents a recent development of RegCM3, a state-of-the-art hydrostatic regional climate model, based on the dynamical core of the mesoscale meteorological model MM5 (Grell et al. 1994), described in detail in Giorgi et al. 1993a, b; Pal et al. 2007. RegCM4 (Giorgi et. al., 2012) includes new land surface, planetary boundary layer, and air–sea flux schemes, a mixed convection and tropical band configuration, modifications to the pre-existing radiative transfer and boundary layer schemes, and a full upgrade of the model code towards improved flexibility, portability, and user friendliness.

Detailed technical details on the model are provided in the deliverable D2.5.1 of the NextDATA project, describing available numerical datasets and models.

Aerosol module in RegCM4

RegCM4 includes a simplified aerosol module, particularly suited for long-term climate simulations, which represents the dynamics of Sulfate, Organic and Black Carbon (OC and BC), desert dust and sea spray. For each of the tracers the aerosol module includes emission sources, transport by resolvable scale winds, sub-grid scale turbulence and deep convection, dry and wet removal processes, simplified chemical transformations, direct radiative forcing both in the solar and infrared spectrum, and a simplified representation of indirect aerosol effects on cloud microphysics. See Qian and Giorgi (1999), Solmon et al. (2005), Zakey et al. (2005) and Zakey et al (2008) for a complete description. Applications include the study the effects of sulfate aerosols on the climate of East Asia (Giorgi et al. 2002, 2003), the effect of desert dust on the west Africa monsoon (Konare et al. 2008; Solmon et al. 2008) and the effects of desert dust storms on the climate of North-East Asia (Zhang et al. 2009). The module provides deposition fluxes of light-absorbing aerosols such as Black Carbon and dust, making it suitable for simulating the effects of aerosol deposition on the snow and the related changes in snow texture and optical properties.

Experimental design

The model has been run by ICTP at 50 km resolution on the standard domain defined for the Indian subcontinent region for the CORDEX project. Three simulations have been performed, in which the external boundary conditions have been provided for present conditions (2000-2009) by the ERA-Interim (ECMWF) reanalysis project and by the CMIP5 EC-Earth 2.3 simulations (performed by CNR-ISAC). A future scenario simulation has been performed in the period 2040-2050 using a RCP4.5 scenario run of EC-Earth 2.3. For the future scenario, CAM large scale aerosol boundary concentrations, and the RCP 4.5 anthropogenic emissions of SO2 and carbon aerosols were used. The oxydant climatology comes from the Mozart CTM (2000-2007). Please see D2.5.1 for a detailed description of the EC-Earth simulations which were used as boundary conditions. Dust and sea salt natural aerosol emissions are computed on-line. The output files are monthly files at 6h frequency and give for each aerosol type the instantaneous concentrations and burden, the average (between two 6h output) deposition fluxes (drydep, rainout, washout), emissions fluxes, the dry deposition velocity. Outputs of AOD and radiative forcings are also available. The emissions from the CMIP5 projects were used for these experiments both for present and for the RCP 4.5 scenario.

Aerosol optical depth

We compare aerosol optical depth (AOD) reproduced by the model simulations with satellite observations available from the Moderate Resolution Imaging Spectro radiometer (MODIS) aboard the Terra satellite. Specifically the Aerosol Cloud Water Vapor Ozone Daily L3 Global 1Deg CMG collection products were used. We also consider an aerosol reanalysis product provided by the MACC (Monitoring Atmospheric Composition and Climate) project (Benedetti et al., 2009), which uses the ECMWF IFS cycle 36R1 model with a prognostic aerosol scheme at resolution T255L60, assimilating MODIS AOD observations. Aerosol reanalysis data are available starting from 1 January 2003.

We gain an insight on the ability of the model to reproduce AOD distributions over the entire region and on the role of long-range transport mechanisms by comparing, in Fig. 4.2.1, climatological averages over the entire simulation domain. While large areas characterized by high albedo, such as the desert areas of Arabia or over the Tibetan plateau in winter, cannot be measured correctly by MODIS, we see that the model presents a good correspondence in the large-scale distribution of AOD. Sulfate emissions in East Asia appear overestimated in the model, and through long range transport may significantly contribute to the presence of increased summer anthropogenic pollutants also over the HKKH. A significant close source area, not seen by MODIS, of dust in summer is evident in the model simulation over western China.

The spatial distributions of the AOD climatologies over the HKKH are reported in detail in Fig. 4.2.2, averaged over the years 2003-2009, common to all datasets.

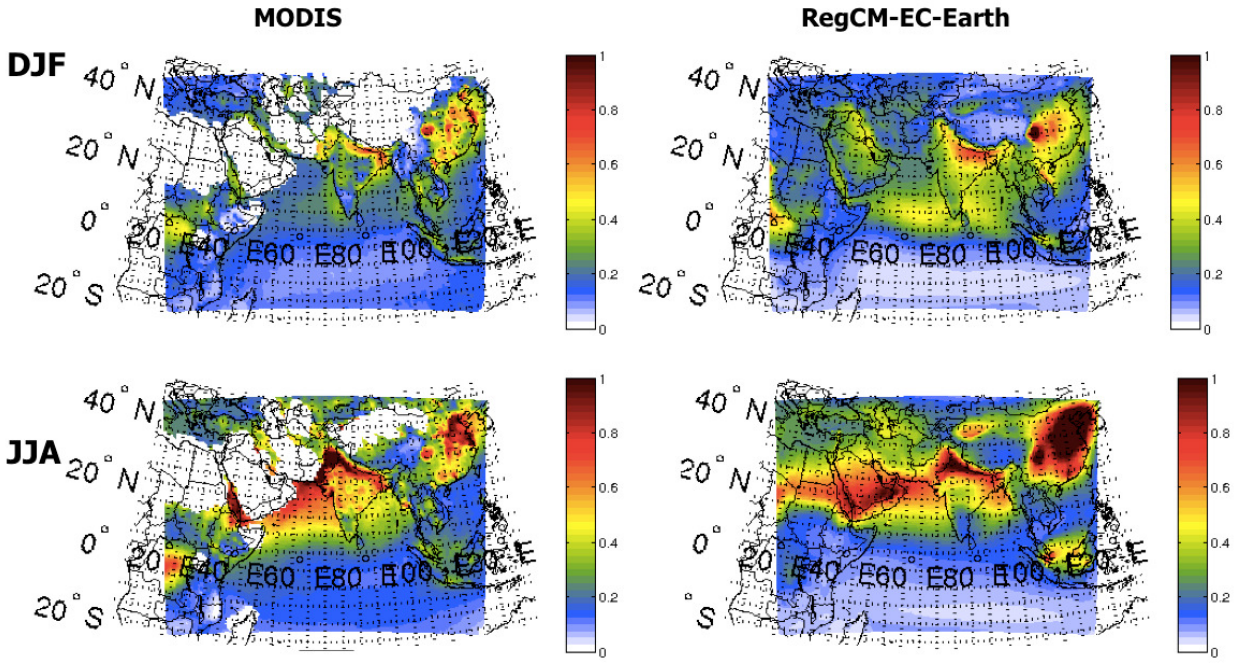

Figure 4.2.1. Large-scale distribution of climatological averages (2000-2009) of AOD in the visible band in MODIS and in the RegCM simulation using EC-Earth boundary conditions.

These figures show that in winter RegCM is capable of reproducing to a large extent the amplitude and the spatial distribution of the optical depth of aerosols in this area, with a good reproduction of a low over the Tibetan plateau and of a higher AOD at the southern feet of the Himalayas, mainly associated with pollution. In summer we find a good reproduction of a severe maximum of AOD centred over the border between Pakistan and India, even if with an offset in the position of the maximum which is located farther east.

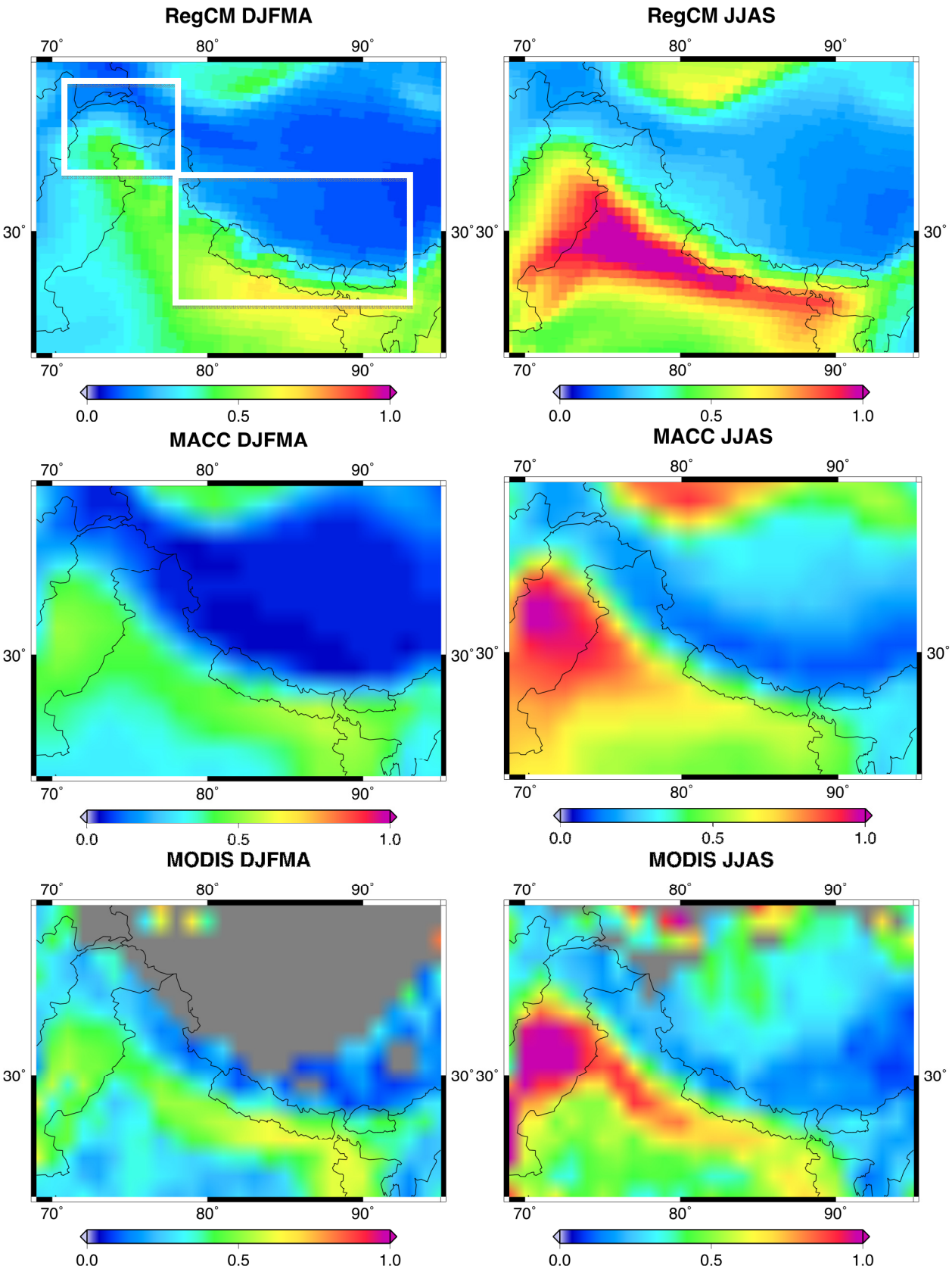

Figure 4.2.2. Comparison over the HKKH of the AOD in the visible band, as simulated by the RegCM4 model with Era-Interim boundary conditions (top row), with the AOD (at 550 nm) reproduced by the MACC reanalysis (middle row) and by MODIS (bottom row). The left column refers to winter-early spring (DJFMA) , the right one to the summer monsoon season (JJAS).

Experimentation with a dynamical dust scheme used in the model has allowed for assessing the role of an accurate representation of dust emissions from the local desert areas (mainly the Thar desert) in order to correctly represent the maximum during the monsoon season. The figure compares the results for present-day conditions using the ERA-Interim reanalysis boundary conditions. Results with EC-Earth boundary conditions are very similar.

A more detailed view of seasonal fluctuations over the two focus areas of the Hindu-Kush-Karakorum (HKK) in the west and over the Himalaya in the east, is obtained by defining two boxes enclosing these areas in the ranges 71E-78E/32N-37N and 78E-93E/25N-32N respectively (shown as white frames in Fig 4.2.2). We report in Fig. 4.2.3 the monthly climatology of AOD over these areas, both for the RegCM model run and for the MODIS and MACC datasets. For the HKK there is a very good agreement in the average AOD in summer, while in winter (from October to February) RegCM reports a significantly higher AOD compared to both MACC and MODIS. Similarly to the two observational databases, RegCM reaches a maximum in July for the HKK. In the Himalaya region MACC and MODIS show a significant difference during all year, which can be attributed to a higher estimate of AOD over the Tibetan plateau in MODIS (see Fig. 4.2.2). While from December to May RegCM AOD maintains itself between these two observational datasets, in summer it reports higher values, which, as we can see in Fig. 4.2.2, are associated with higher AOD over northern India, associated with high dust sources and transport in the monsoon season.

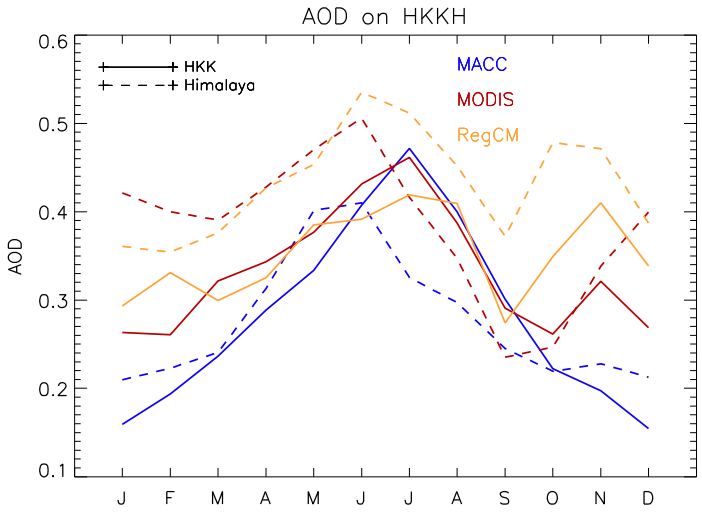

Figure 4.2.3. Monthly climatology of AOD for the HKK and Himalaya boxes defined in the text.

Timeseries of AOD averages over these same regions are reported in Fig. 4.2.4. We see that in the HKK RegCM reproduces well the observed variability and the timing of some extremes of AOD, particularly compared to MODIS. Some high extremes of AOD in winter find no correspondence in the observational and reanalysis datasets. These may be associated with episodes of long-range transport of dust and anthropogenic pollutants which have to be investigated further. In the Himalayas RegCM presents a more irregular timeseries compared to the two observational datasets and is not able to capture some extreme high values observed in summer, particularly by MODIS.

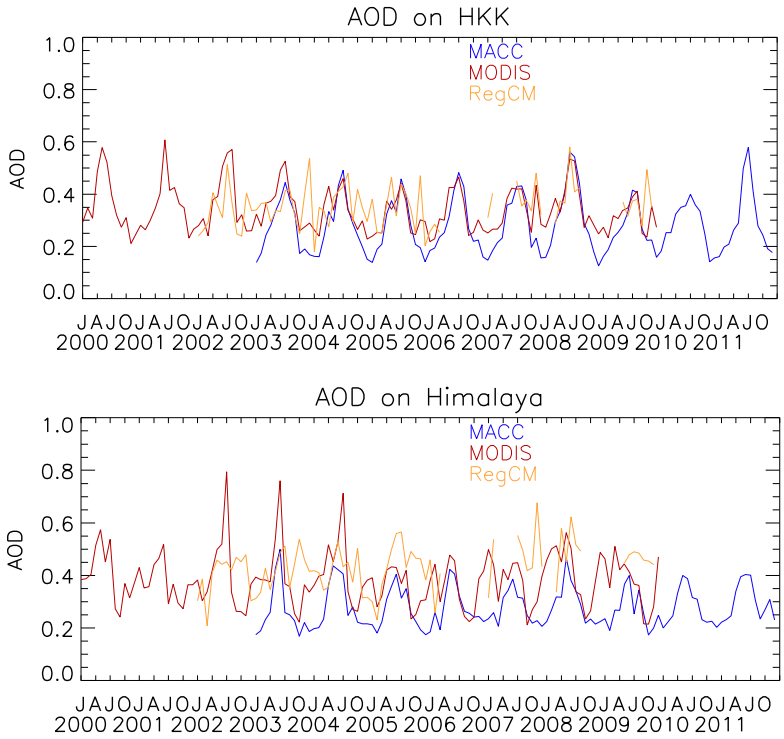

Figure 4.2.4. Timeseries of monthly AOD for the HKK and Himalaya boxes defined in the text.

Deposition fluxes

We analyse the deposition fluxes of light-absorbing aerosols, namely black carbon and dust, in Fig. 4.2.5. This analysis confirms the importance of dust deposition mainly during the monsoon summer season on the southern flanks of the HKKH. The changes in these deposition fluxes in the RCP 4.5 future scenario (for 2040-2050) compared to present-day are shown in Fig. 4.2.6. This analysis highlights a possible decrease in winter BC deposition, mainly associated with a decrease in the scenario of east-Asian anthropogenic emissions. The model also forecasts a significant decrease in dust activity affecting the Himalayas, both in summer (from the Thar desert) and in winter (from the Gobi desert). The associated changes in long-range transport patterns and in wind climatology have to be further investigated, together with possible impacts on snow albedo and local radiative forcing.

3. Summary and outlook

The first year of activity of this pilot study has allowed to prepare and analyse a series of numerical simulations (present-day, with ERA-Interim and EC-Earth boundary conditions, and the RCP4.5 scenario) performed with the RegCM4 regional climate model for the HKKH region. The analysis has confirmed the ability of the model to reproduce the AOD spatial distribution over the focus area and its seasonality compared with MODIS satellite observations and the MACC reanalysis. Analysis of deposition fluxes of light-absorbing aerosols (black carbon and dust) confirms the importance of dust deposition mainly during the monsoon summer season on the southern flanks of the HKKH. Future projections by the model show a significant decrease in dust activity affecting the Himalayas and a decrease in BC deposition.

In the next year of activity the comparison between the model simulations and observations will be extended to available local in-situ observational datasets. In particular AOD and Angstrom parameter measurements available from the AERONET network will be compared.

The analysis will also be extended to other chemical and physical aerosol parameters (such as the aerosol absorption coefficient, concentrations, scattering coefficient, number size distribution, PM1, PM2.5 e PM10) available from the EBAS database parameters and directly from CNR-ISAC, measured at the Nepal Climate Observatory - Pyramid ABC site (Nepal) and measured at sites in the Karakoram range (WP1.1, WP1.2 of the NextData project). Particular interest will be in the analysis of BC and dust long-range transport in the model, identification of source areas and their deposition on snow and ice.

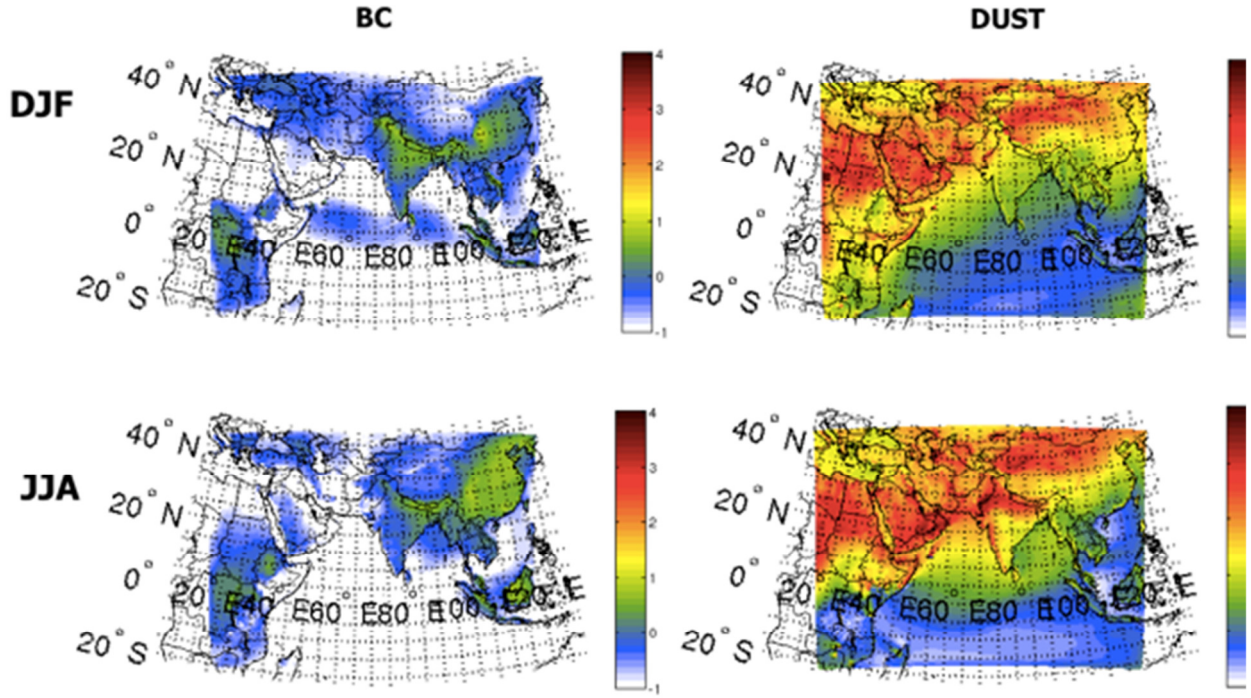

Figure 4.2.5. Aerosol deposition (Log10 of mg/m^2/day) for Black Carbon (left column) and dust (right column) components in RegCM RCP 4.5 present-day simulations.

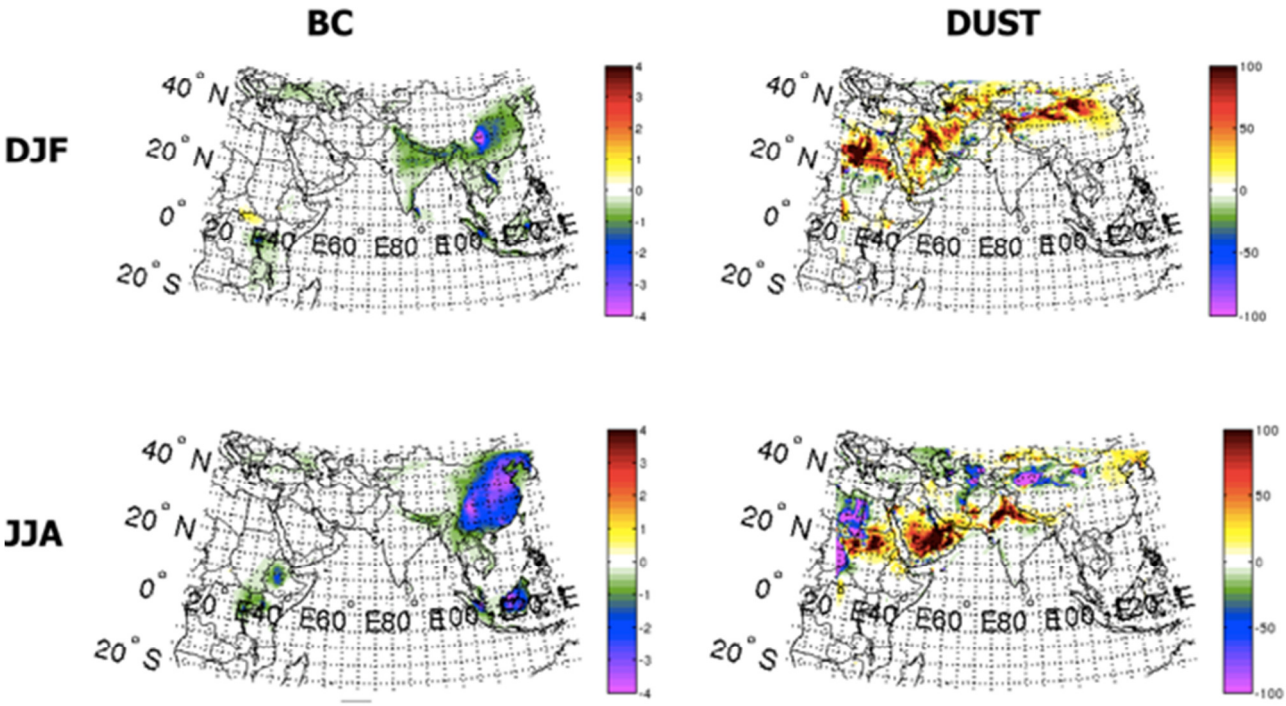

Figure 4.2.6. Aerosol deposition change (Log10 of difference, in mg/m^2/day) for Black Carbon (left column) and dust (right column) components in RegCM RCP 4.5 scenario simulations compared to present day.

Bibliography

Akhtar, M., Ahmad, N., Booij, M. J. (2008), Journal of Hydrology, 355, 148–163. doi:10.1016/j.jhydrol.2008.03.015

Benedetti, A., Morcrette, J.-J., Boucher, O., Dethof, A., Enge- len, R. J., Fisher, M., Flentjes, H., Huneeus, N., Jones, L., Kaiser, J. W., Kinne, S., Mangold, A., Razinger, M., Sim- mons, A. J., Suttie, M., and the GEMS-AER team: Aerosol analysis and forecast in the ECMWF Integrated Forecast Sys- tem. Part II: Data assimilation, J. Geophys. Res., 114, D13205, doi:10.1029/2008JD011115, 2009.

Bonasoni, P.; P. Laj, U. Bonafè, F. Calzolari, P. Cristofanelli, S. Decesari, L.Emblico, MC. Facchini, S. Fuzzi, GP. Gobbi, A. Marinoni, F. Roccato, JM. Pichon, K. Sellegri, H. Venzac, P. Villani, J. Arduini, M. Maione, A. Petzold, M. Sprenger, G. Tartari, GP. Verza and E. Vuillermoz, 2008: The ABC-Pyramid Atmospheric Research Observatory in Himalaya for aerosol, ozone and halocarbon measurements, Sci. Total Env. 391, 252-261.

Clarke, A. D., and J. Noone (1985), Measurements of soot aerosol in Arctic snow, Atmos. Environ., 19, 2045–2054.

Flanner, M. G., Zender, C. S., Randerson, J. T., and Rasch, P. J.: Present-day climate forcing and response from black carbon in snow, J. Geophys. Res., 112, D11202, doi:10.1029/2006JD008003, 2007.

Flanner, M. G., Zender, C. S., Hess, P. G., Mahowald, N. M., Painter, T. H., Ramanathan, V., and Rasch, P. J.: Springtime warming and reduced snow cover from carbonaceous particles, Atmos. Chem. Phys., 9, 2481-2497, 2009

Gautam, R, Hsu, NC, Lau, KM, Tsay, SC, Kafatos, M., Enhanced pre-monsoon warming over the Himalayan-Gangetic region from 1979 to 2007, Geophys. Res. Lett., 36, 2009.

Giorgi F, Marinucci MR, Bates GT (1993a) Development of a second-generation regional climate model (RegCM2). Part I: boundary-layer and radiative transfer processes. Mon Weather Rev 121(10):2794–2813
Giorgi F, Marinucci MR, Bates GT, Canio GD (1993b) Development of a second-generation regional climate model (RegCM2). Part II: convective processes and assimilation of lateral boundary conditions. Mon Weather Rev 121:2814–2832

Giorgi, F., X. Bi and Y. Qian, 2002: Direct radiative forcing and regional climatic effects of anthropogenic aerosols over east Asia: A regional coupled climate-chemistry/aerosol model study. Journal of Geophysical Research, 107, 4439, doi:10.1029/2001JD001066.

Giorgi, F., R. Francisco and J. Pal, 2003: Effects of a sub-grid scale topography and land-use scheme on surface climate and hydrology. Part I: Effects of temperature and water vapor disaggregation. Journal of Hydrometeorology, 4, 317-333.

Giorgi, F., X. Bi and Y. Qian, 2003: Indirect vs. direct effects of anthropogenic sulfate on the climate of east Asia as simulated with a regional coupled climate-chemistry/aerosol model. Climatic Change, 58, 345-376.

Grell, G.A., 1993: Prognostic evaluation of assumptions used by cumulus parameterizations. Monthly Weather Review, 121, 764-787.

Hansen, J., and L. Nazarenko (2004), Soot climate forcing via snow and ice albedos, Proc. Natl. Acad. Sci. U. S. A., 101, 423 – 428, doi:10.1073/ pnas.2237157100.

Hansen, J., and Nazarenko, L.: Soot climate forcing via snow and ice albedos, Proceedings of the National Academy of Sciences of the United States of America, 101, 423–428, doi:10.1073/pnas.2237157100, 2004.

Hewitt, K., 2005, Mountain Research and Development 25, 332–340.

Holland, H. H. and Bitz, C. M.: Polar amplification of cli- mate change in coupled models, Clim. Dynam., 21, 221–232, doi:10.1007/s00382-003-0332-6, 2003.

Immerzeel, W.W., L.P.H. van Beek and M.F.P. Bierkens, 2010: Climate Change Will Affect the Asian Water Towers. Science, 328, 1382-1385.

Konare, A., A.S. Zakey, F. Solmon, F. Giorgi, S. Rauscher, S. Ibrah and X. Bi, 2008: A regional climate modeling study of the effect of desert dust on the West African monsoon. Journal of Geophysical Research, 113, D12206, doi:10.1029/2007JD009322.

Kopacz, M., D. L. Mauzerall, J. Wang, E. M. Leibensperger, D. K. Henze, and K. Singh. 2010. Origin and radiative forcing of black carbon transported to the Himalayas and Tibetan Plateau.ACPD, Vol.10, pp. 21615-21651

Lau, K., M. Kim, and K. Kim (2006), Asian monsoon anomalies induced by aerosol direct forcing, Clim. Dynam., 26, 855–864, doi:10.1007/s00382-006-0114-z.

Menon, S., D. Koch, G. Beig, S. Sahu, J. Fasullo, and D. Orlikowski. 2010. Black carbon aerosols and the third polar ice cap. Atmospheric Chemistry and Physics 10, no. 10: 4559-4571. doi:10.5194/acp-10-4559-2010.

Nigam, S., and M. Bollasina, 2010: The "Elevated Heat Pump" Hypothesis for the Aerosol-Monsoon Hydroclimate Link: "Grounded" in Observations? J. Geophys. Res.

Pal, J.S., F. Giorgi, X. Bi, N. Elguindi, F. Solmon, X.J. Gao, R. Francisco, A. Zakey, J. Winter, M. Ashfaq, F. Syed, J. Bell, N. Diffenbaugh, J. Karmacharya, A. Konare, D. Martinez-Castro, R. Porfirio da Rocha, L. Sloan and A. Steiner, 2007: Regional climate modeling for the developing world: The ICTP RegCM3 and RegCNET. Bulletin of the American Meteorological Society, 88, 1395-1409.

Qian, Y. and F. Giorgi, 1999: Interactive coupling of regional climate and sulfate aerosol models over eastern Asia. Journal of Geophysical Research, 104, 6477-6499.

Ramanathan, V. et al. 2001: Indian Ocean Experiment: An integrated analysis of the climate forcing and effects of the great Indo-Asian haze. J. Geophys. Res. 106, 28371-28398.

Ramanathan, V., C. Chung, D. Kim, T. Bettge, L. Buja, J.T. Kiehl, W.M. Washington, Q. Fu, D.R. Sikka and M. Wild, 2005: Atmospheric brown clouds: Impacts on South Asian climate and hydrological cycle, Proc. Natl. Acad. Sci. 102, 5326-5333.

Solmon F, Giorgi F, Liousse C (2006) Aerosol modeling for regional climate studies: Application to anthropogenic particles and evaluation over a European/African domain. Tellus B 58:51–72

UNEP, 2008: Atmospheric Brown Clouds.

Warren, S. and Wiscombe, W.: A Model for the Spectral Albedo of Snow. II: Snow Containing Atmospheric Aerosols, J. Atmos. Sci., 37, 2734–2745, 1980.

Zakey AS, Solmon F, Giorgi F (2006) Implementation and testing of a desert dust module in a regional climate model. Atmos Chem Phys 6:4687–4704.

Zakey AS, Giorgi F, Bi X (2008) Modeling of seas salt in a regional climate model: Fluxes and radiative forcing. J Geophys Res 113:D14221.

Zhang, D.F., A.S. Zakey, X.J. Gao, F. Giorgi and F. Solmon, 2009: Simulation of dust aerosol and its regional feedbacks over East Asia using a regional climate model. Atmospheric Chemistry and Physics, 9, 1095-1110.